

# We are IntechOpen, the world's leading publisher of Open Access books Built by scientists, for scientists

5,200

Open access books available

128,000

International authors and editors

150M

Downloads

Our authors are among the

154

Countries delivered to

TOP 1%

most cited scientists

12.2%

Contributors from top 500 universities



WEB OF SCIENCE™

Selection of our books indexed in the Book Citation Index  
in Web of Science™ Core Collection (BKCI)

Interested in publishing with us?  
Contact [book.department@intechopen.com](mailto:book.department@intechopen.com)

Numbers displayed above are based on latest data collected.  
For more information visit [www.intechopen.com](http://www.intechopen.com)



# Millennial Oscillations of Solar Irradiance and Magnetic Field in 600–2600

*Valentina Zharkova*

## Abstract

Daily ephemeris of Sun-Earth distances in two millennia (600–2600) showed significant decreases in February–June by up to 0.005 au in millennium M1 (600–1600) and 0.011au in millennium M2 (1600–2600). The Earth's aphelion in M2 is shorter because shifted towards mid-July and longer because shifted to mid January naturally explaining two-millennial variations (Hallstatt's cycle) of the baseline solar magnetic field measured from Earth. The S-E distance variations are shown imposed by shifts of Sun's position towards the spring equinox imposed by the gravitation of large planets, or solar inertial motion (SIM). Daily variations of total solar irradiance (TSI) calculated with these S-E distances revealed TSI increases in February–June by up to  $10\text{--}12\text{ W/m}^2$  in M1 and  $14\text{--}18\text{ W/m}^2$  in M2. There is also positive imbalance detected in the annual TSI magnitudes deposited to Earth in millennium M2 compared to millennium M1: up to  $1.3\text{ W/m}^2$ , for monthly, and up to  $20\text{--}25\text{ W/m}^2$  for daily TSI magnitudes. This imbalance confirms an ascending phase of the current TSI (Hallstatt's) cycle in M2. The consequences for terrestrial atmosphere of this additional solar forcing induced by the annual TSI imbalances are evaluated. The implications of extra solar forcing for two modern grand solar minima in M2 are also discussed.

**Keywords:** Sun: solar activity, Sun: magnetic field, gravitation, solar inertial motion, solar irradiance

## 1. Introduction

Solar activity is usually classified by the numbers of sunspots appearing on the solar surface as locations of magnetic loops generated by electro-magnetic solar dynamo in the solar interior [1] with the number of sunspots on the solar surface to change periodically over an eleven-year cycle [2, 3]. Babcock [4] found that a solar background magnetic field (SBMF) surrounding sunspots has the polarities opposite to the leading sunspot polarities, and these are changing also periodically also every 11 years.

The magnetic polarities of SBF and leading polarities of sunspots are shown to be in anti-phase, e.g. having opposite polarities, as found by comparing solar background and sunspot magnetic fields for cycle 21 [5], and 23 [6]. Furthermore, the SBF was found to be the leading force defining timing and locations of sunspot occurrences on the solar surface and migration to the equator accounting for north-south asymmetry of solar activity [6]. This investigation highlighted the important

role of SBMF in generation of sunspots by dynamo actions and their appearance on the solar surface, thus, defining the solar activity. The link between SBMF (poloidal field) and sunspot (toroidal) magnetic field defines the action of the solar dynamo [1] and it would be beneficial to link a proxy of solar activity to the solar background magnetic field as it is systematically measured in the past 45 years.

Zharkova et al. [7] explored the solar background magnetic field and found the eigen values of the own oscillations of the Sun, by applying Principal Component Analysis (PCA) to the low-resolution full disk magnetograms captured in cycles 21–23 by the Wilcox Solar Observatory. This approach allowed authors to replace a complex magnetic field seen on the solar surface, the photosphere, with the separate wave components, eight plus eigen vectors, which appeared in pairs [8]. The pair of the two principal components (PCs) are the strongest waves of solar magnetic oscillations covering about 67% of the data by standard deviation, with the nearly-equal largest eigen-values, which oscillate with not equal periods of about 11 years [9, 10]. The PCs are shown to be two magnetic waves generated by the dipole magnetic sources produced by the double solar dynamo action [10, 11] in the inner and outer layers of the solar interior [12].

These waves start in the opposite hemispheres while travelling with an increasing phase shift to the Northern hemisphere (in odd cycles) and to the Southern hemisphere (in even cycles) [7, 10]. The summary curve of these two waves is found close to the averaged sunspot numbers, which define the current solar activity index [9, 10]. This summary curve of solar magnetic waves is proposed as a new proxy of solar activity, which allows us to predict solar activity on any timescale and also to add a magnetic polarity of the background field for a given cycle, known to be opposite to leading polarity of sunspots [6]. The maximum of solar activity for a given cycle (or double maximum for the double waves with a larger phase shift) occurs at the times when each of the waves approaches its maximum, so that at the equal amplitudes the two waves can have a resonant interaction, naturally accounting for often-reported North–South asymmetry of solar activity [6, 13–15].

In order to test further predictions of solar activity with the summary curve of two magnetic waves generated by double dynamo in the Sun in two layers, the summary curve was extended using the mathematical formula from the current time forwards to 3200 and backwards to 1200 [10] (see **Figure 1**). This led to a discovery of grand solar cycles (GSCs) of solar activity with a duration of 350–400 years, evidently caused by the interference (beating effect) of the two magnetic waves with close but not equal frequencies [10]. There were far fewer sunspots seen during some periods, for example, during the Dalton minimum (1790–1820), and practically none during the period known as the Maunder minimum (1645–1715) [16]. Such dramatic reductions in solar activity, which are longer than a single eleven-year sunspot cycle, are known as grand solar minima (GSMs).

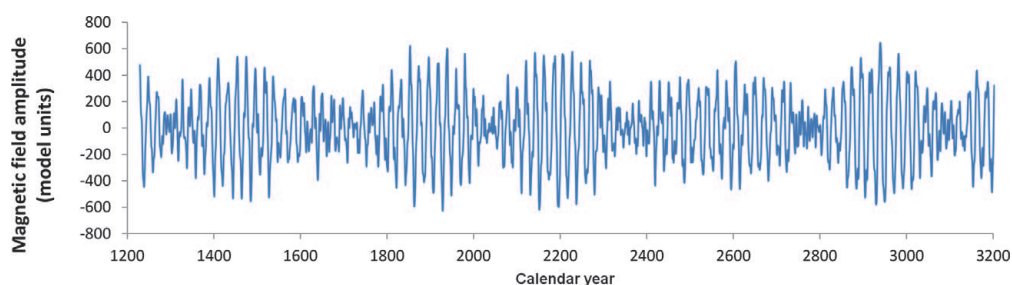


**Figure 1.**

*The summary curve (in arbitrary units) of solar activity calculated for 1200 to 3200 years from the 'historical' period (1976–2008, cycles 21–23). Positive magnitudes of the summary curve represent northern magnetic polarity while the negative ones - southern magnetic polarity. Reproduced from the data of Zharkova et al. [10].*

The timings of previous GSMs are found to closely fit the Maunder minimum (1645–1715) [16] and Wolf minimum (1280–1350), and to predict the two upcoming modern GSMs (2020–2053 and 2375–2415). Furthermore, by extrapolating the summary curve backwards to 1000 BC the further GSMs are fit by the curve: Oort’s (1040–1080), Homeric (780–710 BC) and many others [17]. This restoration of summary curve [17] clearly gives a better accuracy of solar activity definition, in comparison with the prediction of sunspot activity restored from the past TSI derived with carbon-14 isotope dating [18].

Then, as the next step, Zharkova and co-authors [19] derived the magnitudes of a baseline (zero-line) magnetic field for each 22-year sets and discovered rather rigid periodic variations of this baseline magnetic field with a period of about 2000–2100 years. This period resembles the period of 2200 years of Hallstatt’s cycle reported from the restoration of solar irradiance in the Holocene [20–22]. It is rather difficult to find any mechanism in the solar interior that can account for much weaker and longer oscillations of the baseline of magnetic field. This led us to look for a some kind of periodic forcing linked to the orbital motion of the planets.

Jose [23] first suggested that solar activity on a longer timescale can be affected by the motion of large planets of the solar system. This suggestion was later developed by many researchers (see for example [24–27]) who found that the Sun, as a central star of the solar system, is a subject to the inertial motion around the center-of mass, or barycentre, of the solar system induced by the motions of the other planets (mostly large planets, e.g. Neptune, Jupiter, Saturn and Uranus).

Solar inertial motion (SIM) is the motion of the Sun around this barycenter of the solar system inside the circle with a diameter of about  $\Delta = 4.3R_{Sun}$ , or  $\Delta = 4.3 \times 6.95 \cdot 10^5 = 2.9885 \cdot 10^6$  km, where  $R_{Sun}$  is a solar radius as shown in **Figures 4** and **5** in [19] reproduced from [27, 28]. This schematic drawing (see Fig. 4 in [19]) illustrates sudden shifts in the Sun from the location in the ellipse focus, where it is supposed to reside by Kepler’s laws, because the Sun travels in an epitrochoid-shaped orbits about the center-of mass (barycentre) of the solar system.

The SIM orbits are induced the tri-fall positions of large planets achieved for different planet configurations changing approximately within different periods of 370 or 2200–2400 years related to the planet positions and their rotation around the Sun [29, 30]. Hence, a joint effect of the orbital effects introduced by the combined motion of the Earth on the orbit and the Sun about the barycentre of the solar system can be the important factors in defining the observed long timescale variations of solar irradiance at the Earth and terrestrial temperature, which has not been explored yet, despite the Sun is the main source of energy of all the planets.

Solar irradiance is accepted to be one of the important factors defining temperature variations on the Earth and other planets as it is the main source of the energy for all planets. During the Maunder minimum, solar activity was significantly reduced for six solar cycles of 11 years and so was the terrestrial temperature in the

Authors	Maunder minimum	2000–2012
Lean et al.1995 [31]	1363	1366
Steinhilber et al., 2012 [22]	1364	1366
Shirley et al., 1990 [26]	—	1370
Wolff and Hickey, 1987 [32]	—	1371
Lee et al., 1985 [33]	—	1372

**Table 1.**  
 The solar irradiance in  $W/m^2$  restored and measured since Maunder minimum.



Northern hemisphere. This was considered to be a result of a reduction of solar irradiance during the Maunder Minimum.

More recent reconstruction of the cycle-averaged solar total irradiance back to 1610 suggests that since the end of the Maunder minimum in 1710 until 2010 there was the increase of the irradiance by a magnitude about  $1 - 1.5 \text{ W/m}^2$  [34]. This increase is correlated somehow with the increase of the baseline terrestrial temperature since the Maunder minimum (e.g. recovering from the little ice age) [35]. Although, it is not clear yet if this trend in variations of the terrestrial temperature and solar irradiance is caused by the increased solar activity itself, which, in fact, started to decrease in the past decades, or by some other factors of the solar-terrestrial interaction and by human activities, or by the combination of all the three factors.

In the current chapter we analyse the observational variations of Sun-Earth distances derived from the published ephemeris in the two millennia 600–2600 and relate them to the variations of solar irradiance at the Earth and explore their possible links oscillations of the baseline solar magnetic field and with the reported planetary motions.

## **2. Observed millennial oscillations of solar irradiance and baseline solar magnetic field**

### **2.1 Millennial oscillations of solar irradiance**

Reconstruction of cycle-averaged total solar irradiance (TSI) back to 1610 suggests an increase of the solar irradiance by a value of about  $3 \text{ W/m}^2$  (see **Figure 2**) [31, 39], or about 0.22% of the total solar irradiance since the end of the Maunder minimum (see **Figure 2**, left plot).

The space observations in 80s of the total solar irradiance obtained by NIMBUS 7 instruments show pretty wide range of magnitudes varying up to  $1370 \text{ W/m}^2$  [26], to  $1371 \text{ W/m}^2$  [32] or  $1372 \text{ W/m}^2$  [33]. The wide variety of the measured magnitudes of solar irradiance indicates that this physical parameter from the Sun is not as constant as many researchers assume. Although, these changes of solar irradiance from the MM until present times are, in general, small, compared to the tens of watts occurring during seasonal and latitude differences, which may have a noticeable impact on the Earth temperature.

Note, we do not include in this comparison the most recent restorations of the solar irradiance [34, 40], who considered the re-normalised solar irradiance after Maunder minimum and used a magnetic flux transport model with strongly averaged past solar magnetic fields, which make rather difficult to compare these magnitudes of solar irradiance with the non-normalised early observations.

The variations of the solar irradiance recovered for the Holocene from the variations of the carbon  $^{14}\text{C}$  isotope abundance in the terrestrial biomass [37] (see **Figure 3**, top plot), demonstrate weak oscillations with a period of about 2200 years, or Hallstatt's cycle [20, 21], which are imposed onto the longer-term (16-20 K years) orbital oscillations (possibly, one of Milankovich cycles) [41, 42]. The solar irradiance oscillations restored over the past 12 000 years [20, 43] were also tested with the wavelet transform spectral analysis, which clearly demonstrate the similar period of 2200 years [22] or up to 2400 years [44]. These baseline oscillation periods are very close to the 2200 year period called Hallstatt's cycle reported from the other observations of the Sun and planets [21, 22, 24, 45].

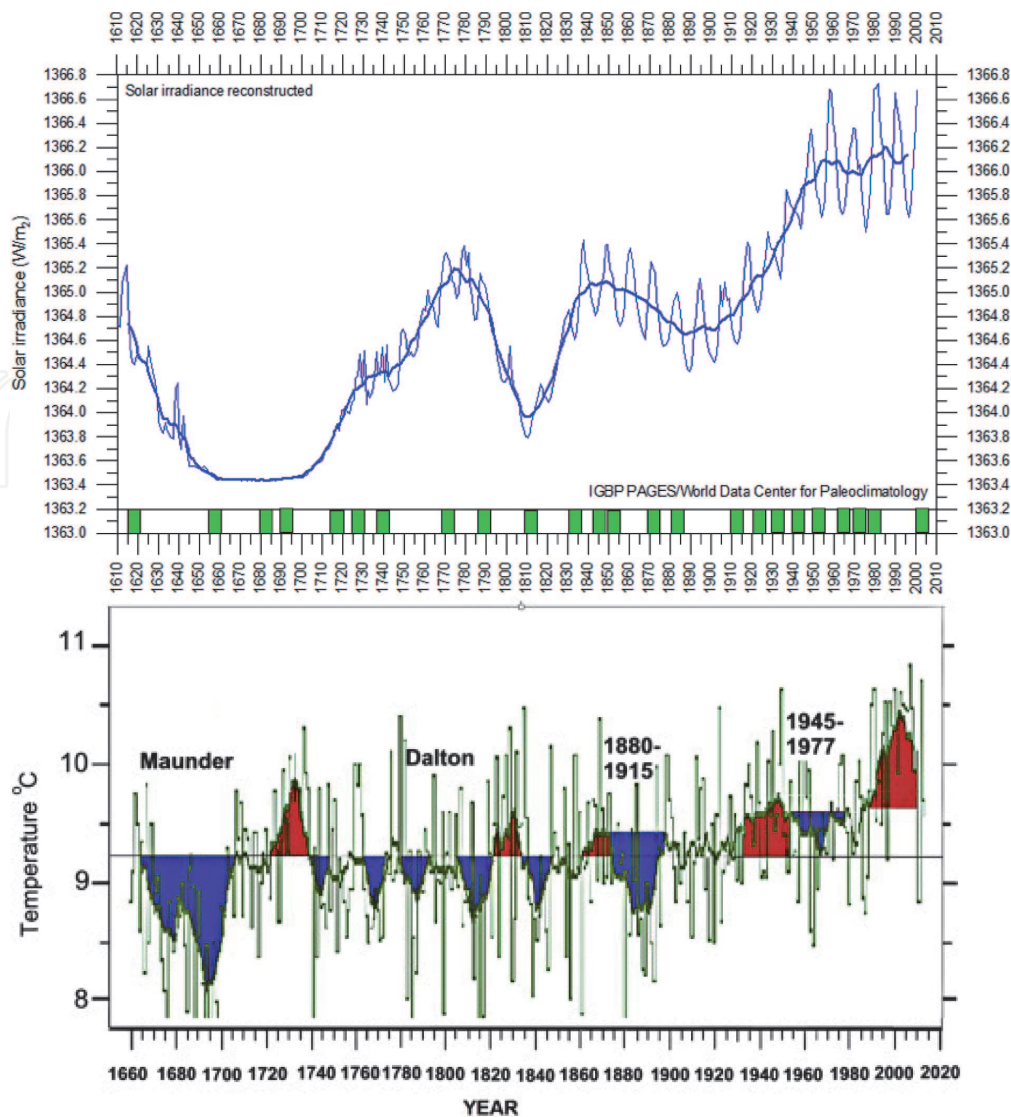


**Figure 2.**  
 The variations of solar irradiance (left) [31] and terrestrial temperature (right) [36] recovered from the Maunder minimum, which demonstrates a significant drop of the solar irradiance and terrestrial temperature during the previous GSM, Maunder minimum (see the text for details).

## 2.2 Millennial oscillations of the baseline magnetic field

Recently, Zharkova et al. [19] reported the similar millennial oscillations of the baseline (zero-line) of the solar background magnetic field (SBMF) calculated from the summary curve obtained with Principal Component Analysis (PCA) [10]. The baseline magnetic field is defined from filtering out large-scale 22 year oscillations, or finding the mean point between two 11 year cycles for the expanded summary curve of 120 thousand years. As result, we detect weak two millennial oscillations of the SBF baseline with a period of  $2000 \pm 95$  years [19] shown by the navy curve in **Figure 3** (bottom plot). Although, the scale of these baseline oscillations is much smaller (ranging from  $-10$  to  $10$ ) than the 11 year magnetic field variations of the summary curve (ranging in  $-400,400$ ) that is shown in **Figure 3** (bottom plot) for the redacted summary curve (cyan curve) calculated backwards between 70 and 90 thousand years [19]. Note, the summary curve presented by cyan curve in **Figure 3** (bottom plot) has different appearance from that in **Figure 1** (top plot) [19] because it was redacted to a single point per year instead of 13 points (for Carrington rotations) originally used [10, 17].

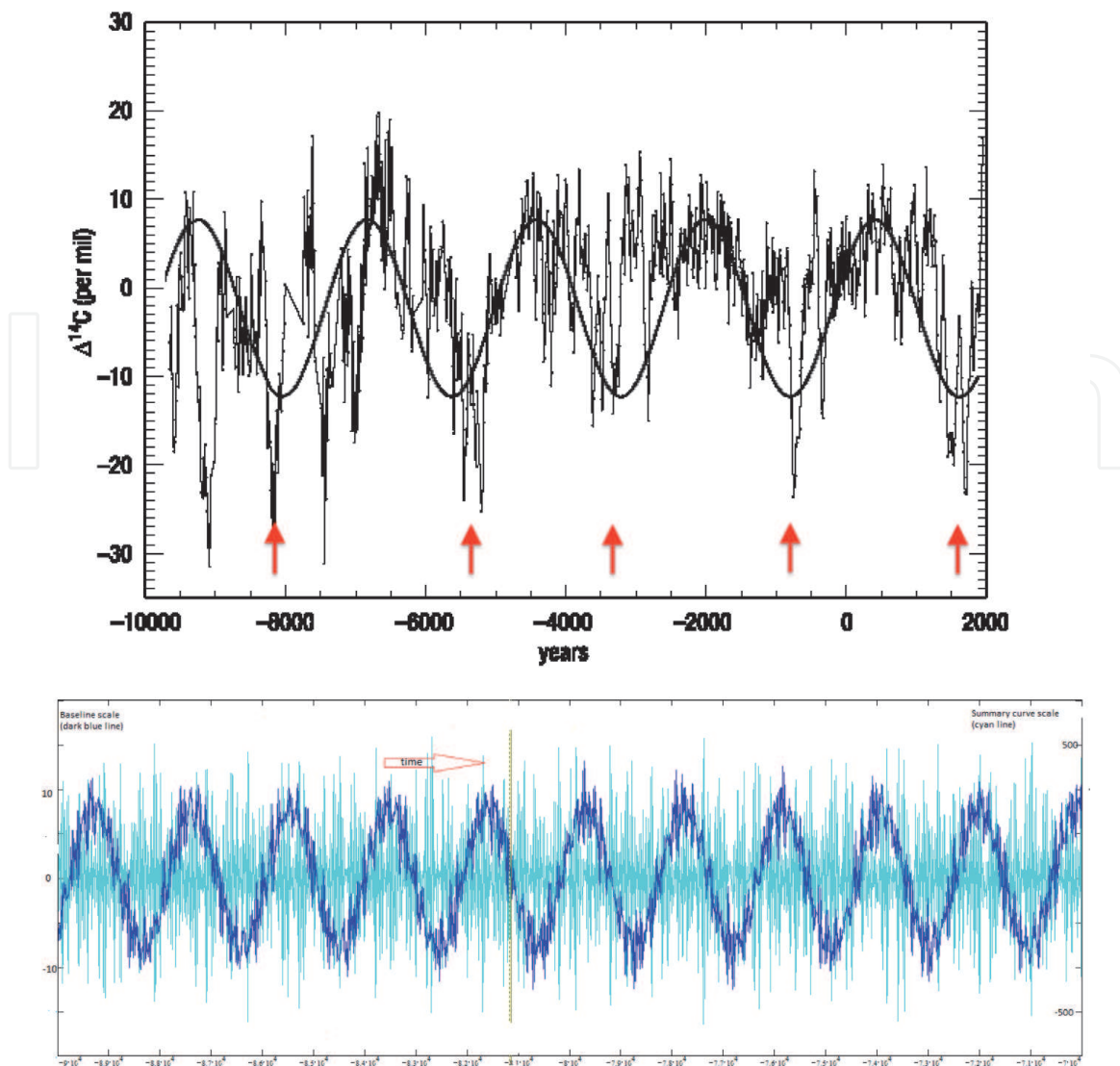


**Figure 3.**

Top plot: The millennial oscillations with a period (2100–2200) (Hallstatt cycle) of the carbon  $^{14}\text{C}$  isotope abundances reported in parts per thousand (per mille, %) used for solar irradiance dating in the IntCal09 data from Reimer et al. [37]. This period is similar to that derived from the solar irradiance restored in the past 12,000 years with a wavelet transform by Steinhilber et al. [22] (see their Figure 4). The positive sign means excess and the negative sign means deficit of abundances. Bottom plot: The oscillations of the baseline (zero line, see for details section 2.2) of solar background magnetic field (left Y axis, arbitrary units, navy line) with a period of about  $2000 \pm 95$  years over-plotted on the oscillations of the reduced summary curve (right Y-axis, arbitrary units, cyan line). Positive magnitudes of the summary and baseline curves represent northern magnetic polarity while the negative ones – southern magnetic polarity. Adopted from Zharkova et al. [19].

Hence, the baseline magnetic field in Figure 3 (bottom plot) reveals the very stable oscillations with a period of  $T_{base} = 2000 \pm 95$  years [19]. Evidently, these baseline oscillations are normally incorporated into the magnetic field measurements of the summary curve (cyan curve) and, thus, are not detected in the unfiltered observations. The baseline oscillations of magnetic field have a very stable period maintained during the whole duration of simulations of 120 thousand years meaning these oscillations of the baseline magnetic field on a millennial timescale to be induced by a rather stable process either inside or outside the Sun.

The variations of the magnetic field baseline oscillations for the current Hallstatt's cycle are shown in Figure 4 (top plot, navy line) (from [19]) indicating that it started at Maunder minimum and is in ascending phase now [20, 43] and the reduced summary curve of magnetic field (cyan line). The irradiance curve was reduced in magnitude by factor 3, in order to distinguish this curve from the



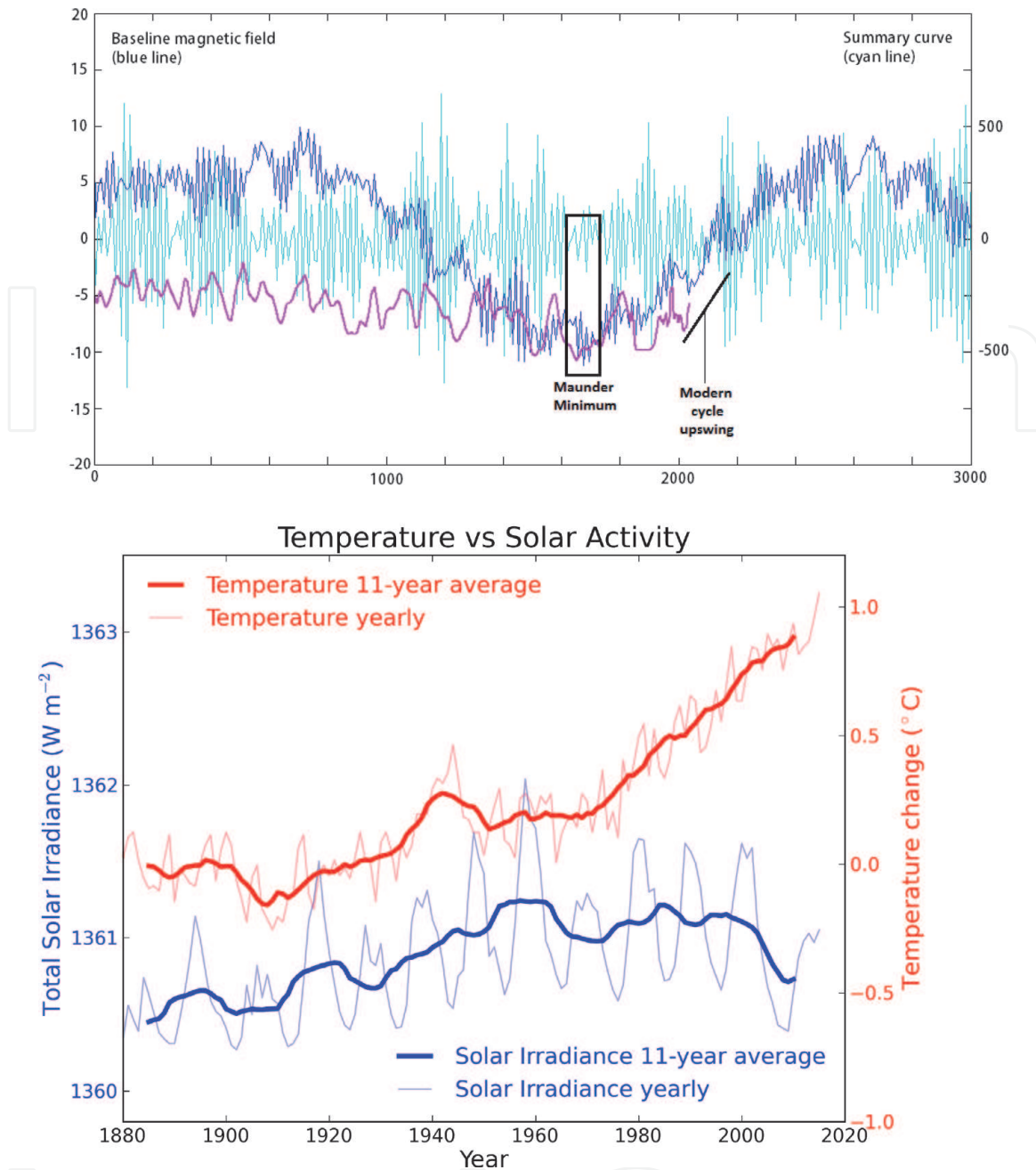


**Figure 4.** Top plot: The close-up view of the current cycle of the baseline magnetic field (dark blue curve, arbitrary units, see for details section 2.2) with the minimum occurring during Maunder minimum. The scale of the baseline variations are shown on the left hand side of Y axis, the scale of the summary curve variations - on the right hand side Y-axis. The irradiance curve (magenta line) taken from [20, 37], their **Figure 3** (top plot), over-plotted on the summary curve of magnetic field (cyan curve) [19]. The irradiance curve had to be reduced in magnitude to avoid full overlapping with the baseline magnetic field curve. The black line defines the slope of the baseline terrestrial temperature from [35]. Adopted from Zharkova et al. [19]. Bottom plot: The variations of terrestrial temperature (red lines) and total solar irradiance (measured in W/m<sup>2</sup>) (blue lines) during each solar cycle (thin lines) and the one averaged per cycle (thick lines) derived by [38].

baseline oscillations (e.g. Spearman's correlation coefficient between these two curves is about 0.68). After the MM the magnetic baseline curve is growing towards northern polarity, while the solid dark line showing the rate of increase of the baseline terrestrial temperature [35].

From the close-up plot of the current millennial baseline cycle in **Figure 4** (top plot) it becomes evident that from 1600 the baseline magnetic field was shifting towards the northern polarity approaching its maximum in about 2600. This increase of the baseline magnetic field of northern polarity is likely to coincide with the increase of solar irradiance curve [20, 43]. The baseline terrestrial temperature



curve is shown increasing by  $0.5^{\circ}\text{C}$  per 100 years [35] and has a slope (shown by the black line in **Figure 4** top plot) close to that of the magnetic field baseline increase (navy line) [19]. At the same time, the variations of the terrestrial temperature versus solar activity shown in **Figure 4** (bottom plot) [38] reveal that in the past few decades the Earth temperature increase goes against the solar activity showing the signs of decrease. This raised some reasonable questions about the cause of the terrestrial temperature increase and led to suggestions of substantial extra-heating of the Earth atmosphere caused by greenhouse gases.

### 3. Millennial variations of the sun-earth distance

The observations of solar irradiance and magnetic field baseline oscillations with the period of about 2100–2200 years are believed to be imposed on the Sun by the gravitational effects of Neptune and Saturn causing SIM [30, 46]. In this section we carry out the investigation of Sun-Earth distance variations over a millennial scale in an attempt to establish if they follow or deviate from Kepler's laws.

#### 3.1 Ephemeris of the sun-earth distances in 600–2600

Let us now explore the daily Sun-Earth (S-E) distances over the two millennia (600–2600) derived from the ephemeris of VASOP87 - Variations Seculaires des Orbites Planetaires [47] [http : //neoprogrammics.com/vsop87/planetary\\_distances/tables/](http://neoprogrammics.com/vsop87/planetary_distances/tables/). Note that the VSOP87 data up to 6 digits after the decimal coma coincide with the widely used JPL ephemeris [48].

The daily Sun-Earth distances for every month of the three years for each millennium: M1 (600, 1100, 1600) and M2 (1700, 2020, 2600) are presented in **Figure 5** (January–June) and **6** (July–December) for the millennia M1 (600–1600) (left column) and millennium for M2 (1600–2600) (right column). The Sun-Earth distances change rather differently over the two millennia M1 and M2 from what one would expect from the elliptic motion of the Earth about the Sun where the perihelion (shortest distance) and aphelion (longest distance) occur on the semi-major axis of the ellipse and the distances are defined by Kepler's third law (see **Figure 15** and Eq. (6) in Appendix A).

However, instead of it, one can observe a significant reduction of the Sun-Earth distances in January–June (**Figure 5**) and their increase in July–December (**Figure 6**). Furthermore, the maximal differences, or differences between the S-E distances at the start and end of each millennium considered presented in **Figure 7**, reveal these maximal differences reaching 0.005 au in April–May (**Figure 5**) in millennium M1 and up to 0.011 au in April–May in millennium M2. These are followed by significant increases of the S-E distances in August–December shown in **Figures 6** and **7**. Moreover, the daily double differences, e.g. the differences between the maximal differences of the S-E daily distances in M1 and M2, taken from **Figure 7**, plotted in **Figure 8** demonstrate that in March–June there is a large reduction of the S-E distances in M2 compared to M1.

In order to evaluate if these changes are symmetric, let us present the mean monthly S-E distance variations during each sample year considered plotted in **Figure 9**. This, in fact, reveals that in M1 the increases/decreases of the S-E distances (left plot) are nearly symmetric over each year and centred about the summer solstice in June and winter solstice in December while in the millennium M2 the distance curve is skewed (right plot) with the maximal Sun-Earth distances being noticeably shifted in time towards a mid-July for aphelion and mid-January for

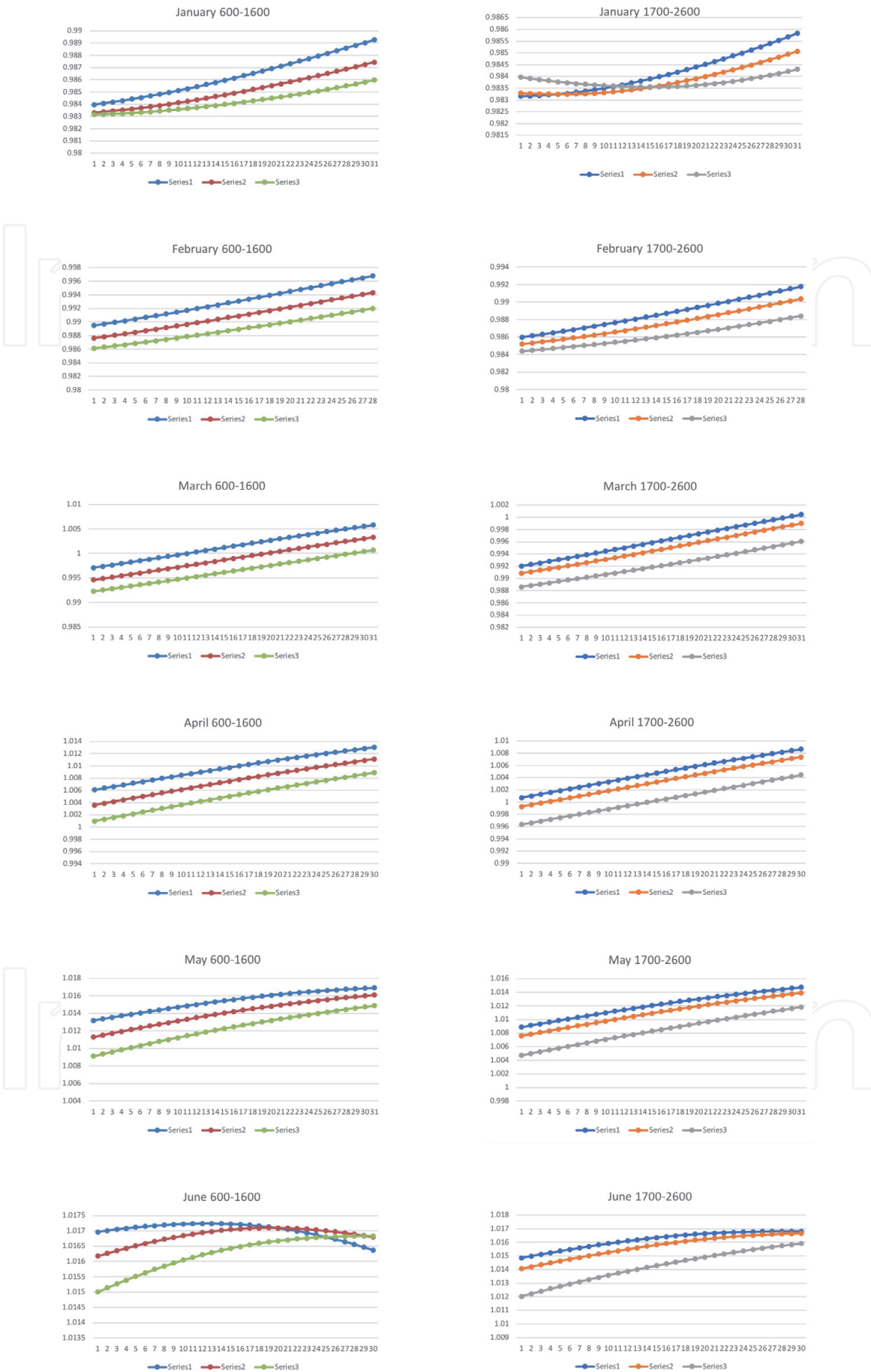


**Figure 5.** Variations of the sun-earth distances (in astronomical units, au) versus days of the month (X-axis) in January–June for three sample years in the millennium M1 (600–1600) (left) and M2 (1600–2600) (right). Left column: Blue - year 600, red –1100 and green –1600; right column: Blue - year 1700, red - 2020 and grey - 2600.

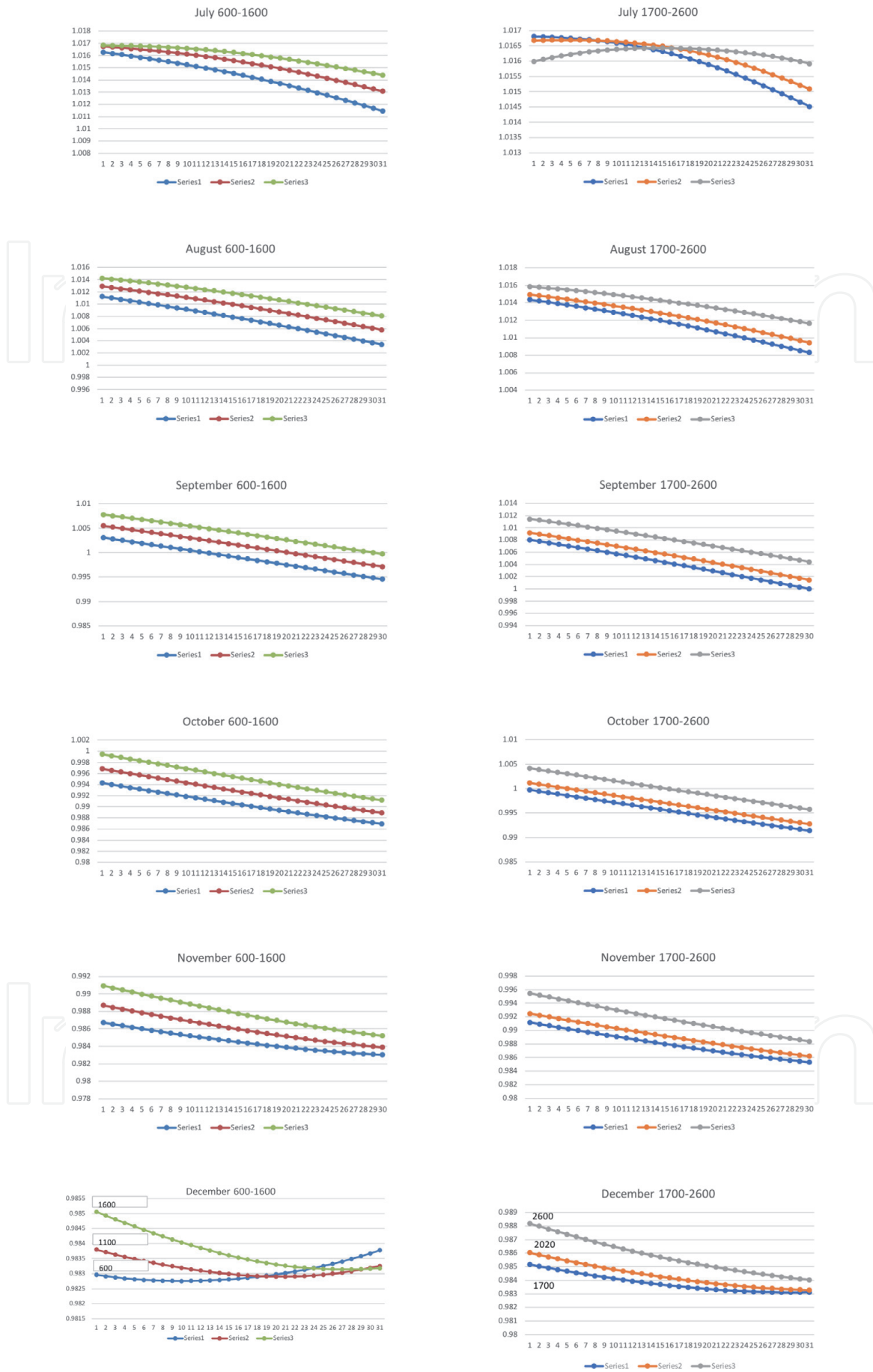


**Figure 6.** Variations of the daily sun-earth distances (in astronomical units, au) versus days of the months in July–December of three sample years selected in the millennium M1 (600–1600) (left) and M2 (1600–2600) (right. Left column: Blue - year 600, red –1100 and green –1600; right column: Blue - year 1700, red - 2020 and grey - 2600.

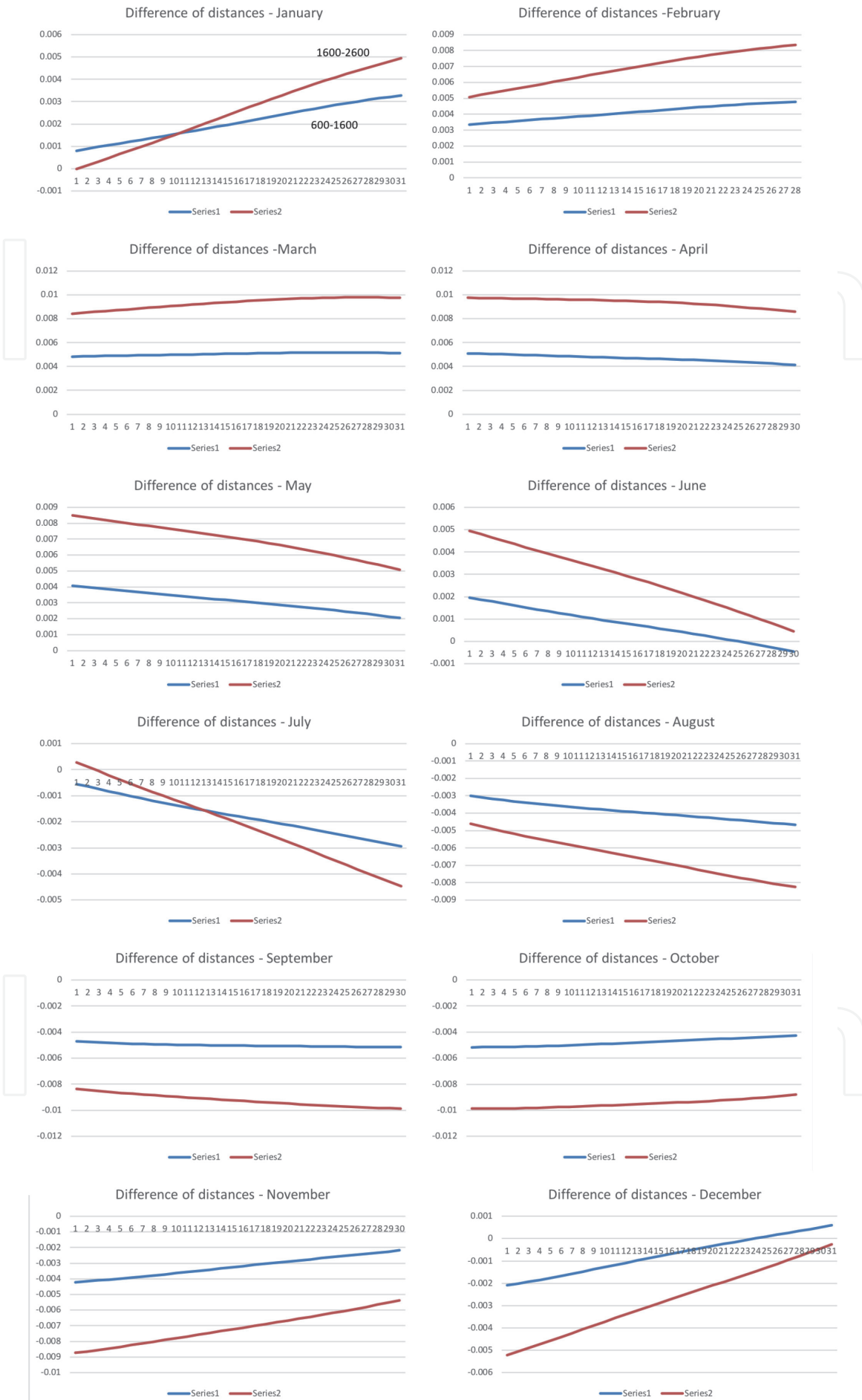


**Figure 7.** Maximal daily differences for each months of the sun-earth distances (in astronomical units, au) between the years 600–1600, M1 (blue curves) and 1700–2600, M2 (red curves). X-axis shows days of the months.



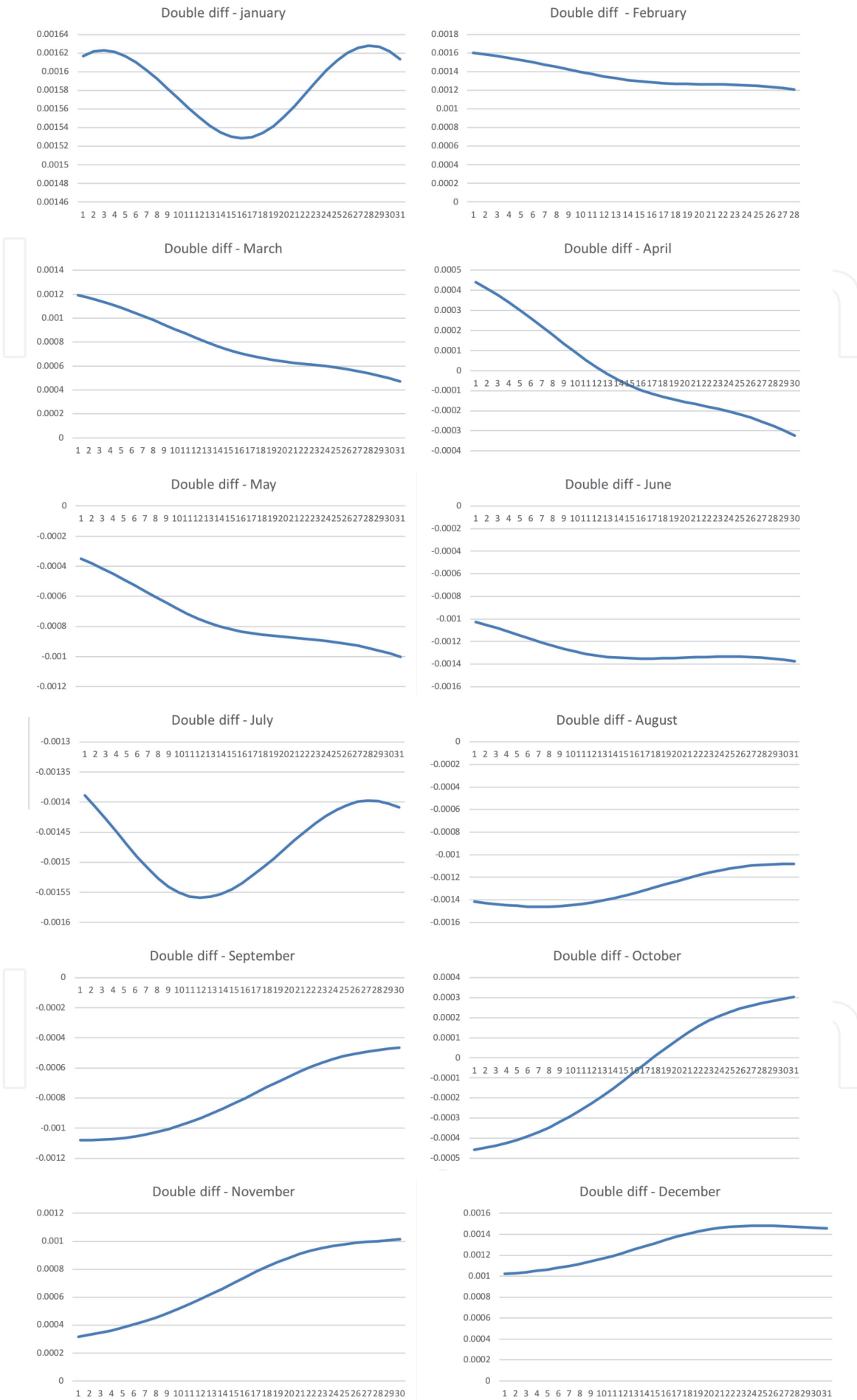


**Figure 8.** The differences between the maximal variations of the daily sun-earth distances (in astronomical units, au) in millennium M1 (600–1600) and M2 (1700–2600) shown in **Figure 7**. X-axis shows days of the months.

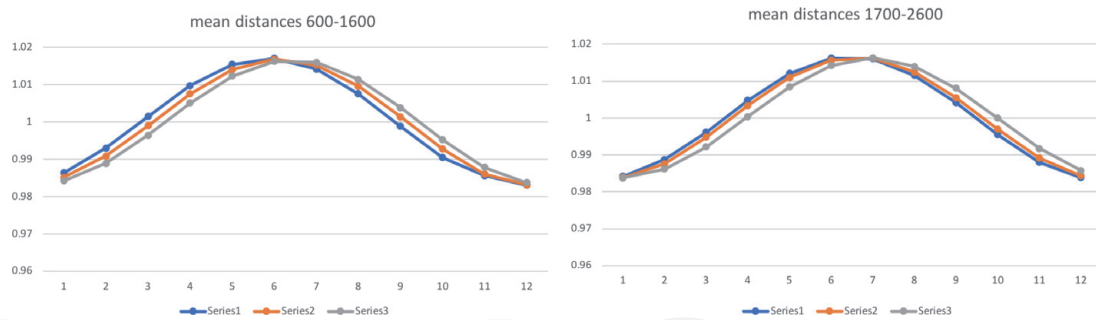


**Figure 9.** Variations of the annual sun-earth distances (in astronomical units, au) versus months of the year in the millennia M1 (left) and M2 (right). Left plot: Blue curve - year 600, red curve -1100 and grey curve - 1600; right plot: Blue curve -1700, red curve - 2020 and grey curve - 2600.

perihelion. Namely, in M1 the local perihelion and local aphelion are shifted forward by 5–6 days to 26–27 December and 26–28 June, respectively, from the summer and winter solstices on 21 June and 21 December accepted for elliptic orbit of the Earth revolution about the ellipse focus. While in M2 the local perihelion and aphelion in 2600 are shifted from the elliptic orbit positions for the winter and summer solstices forward by up to 25–26 days (to 15–16 January and 15–16 July, respectively, seen in the right column of **Figures 5 and 6**.

This asymmetry in the changes of the S-E distances in M2 compared to M1 is more clearly demonstrated by the annual variations of the double differences between the S-E distance shown in **Figure 8** after they are averaged for each month and presented over a year in **Figure 10** for each sample years considered. It clearly shows that the shifts in the S-E distances are reduced more in the April–September and increase more in October–February of each year of millennium M2. This means that the input of solar irradiance to the Earth is not evenly distributed over time of the Earth revolution, or over the Earth location on the orbit.

### 3.2 Proposed interpretation of the S-E distance variations

If the Earth revolves about the Sun located in the focus of the ellipse, the Sun-Earth distance has to change depending on the Earth position on the orbit following Kepler's 3rd law (see Eq. 6 in Appendix A). Earth orbit is a stable elliptic orbit with little changes of the major and minor axis, as established in Appendix C with the help of Appendices A and B. However, the S-E distance reductions and growths reported here deviate from the Kepler's third law (Eq. 6 in Appendix A). By

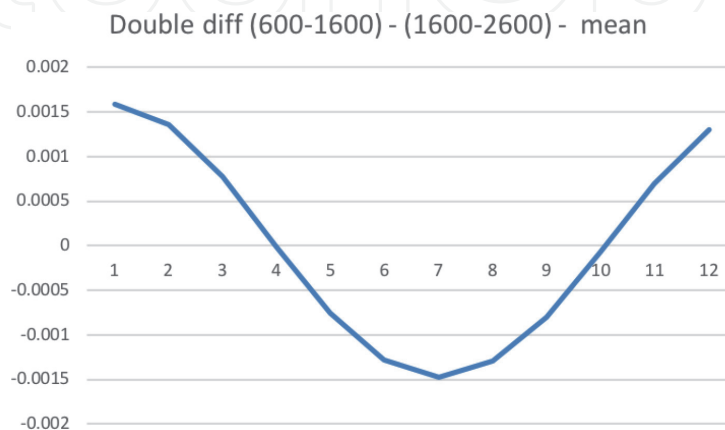


**Figure 10.** Annual variations of the differences between the mean maximal monthly differences in the sun-earth distances (in astronomical units, au) in millennium M1 (600–1600) and M2 (1700–2600) taken from **Figure 8**. Axis X shows months of a year.

comparing the mean-by-time and mean-by-arc S-E distances for an elliptic orbit (see Appendices B) with the expected changes imposed by the calculated shifts of aphelion and perihelion [51] shown in Appendix C, it is evident that the real S-E distances derived from the ephemeris are different from Kepler's 3rd law (see Eq. 6 in Appendix A).

This can only happen if these S-E ephemeris reflect the additional motion: the revolution of the Sun about the barycentre, which is induced by the action of large planets of the solar system. The similar effect is observed in the stars, which have planetary systems, leading to a wobbling star effect that is used to trace possible exoplanets [52, 53]. The shift of S-E distances reported above should be caused by the increasing shift of the Sun's location from the focus of the ellipse, where it is supposed to reside, according to Kepler's laws, towards the spring equinox of the Earth orbit. This shift of the position of the Sun with respect to the barycentre has been recognised as the solar inertial motion - SIM [25, 27, 30]. The resulting S-E distances are defined by the superposition of these two motion: Earth revolution and SIM.

In fact, the variations of the S-E distances during the two millennia are likely to be affected by the gravitational effects of Jupiter, Saturn, Uranus and Neptune on the Sun's inertial motion [30] revealing the oscillations of the planet orbits with a period of 8.5 thousand years (see Fig. 1 in [30], affecting SIM. From the whole period of 8.5 thousand years reported in the paper the semi-period with maximum of 4.2–4.3 thousand years with the ascending part of 2.1 thousand years are similar to the period of decreasing S-E distances reported in section 3.1 for 600–2600. Also the reported S-E distances reveal the noticeable shifts of the aphelion and perihelion from the major axis of the ellipse that coincides also with the oscillations of magnetic field baseline [19, 49] and solar irradiance [22]. It seems that in the two millennia 600–2600 the large planets continuously shifted the Sun from its focus towards the spring equinox as detected from the S-E ephemeris in **Figures 5 and 6**.

Therefore, it can be noted that owing to SIM, the shortest and longest Sun-Earth distances (perihelion and aphelion) in the elliptic orbit of the Earth are shifted to the local aphelion and perihelion, which are located on the shorter axis of the ellipse than the major axis. This line has an angle  $\phi$  to the semi-major axis roughly defined by the formula for  $\tan \phi$ :

$$\tan \phi = \frac{2d_s}{f}, \quad (1)$$

where  $f$  is a distance between the foci of the ellipse and  $d_s$  is the shift along the semi-minor axis  $b$  of the Sun from the focus of the ellipse. Naturally, by the definition of an ellipse, this line is shorter than the semi-major axis  $a$  of the Earth elliptic orbit, which is the longest axis in the ellipse.

Furthermore, the calculations of the double differences between the maximal distance shifts occurred in millennia M1 and M2 (M1-M2) for daily data shown in **Figure 8** and their annual variations shown in **Figure 10** reveal that the double differences become negative in April and remain such until the end of October. This means that in M2 (1600–2600) the S-E distance decreases in April–July and its increases in July–December are much larger than in M1 (600–1600). This also indicates that in M2 the Sun becomes closer and closer to the Earth during April–October before the Earth revolution will make the S-E distance increases in November–February, since these increases are larger than expected from Kepler's third law. This, in turn, can lead to a significant solar radiation input to the Earth in millennium M2, which needs to be processed by the Earth atmosphere and ocean that will be discussed below in section 4.

These long-term SIM effects can explain the reported above significant S-E distance decreases in January–June and the similar increases in July–December during the both millennia. The magnitudes of the S-E distance oscillations are smaller for M1 (up to 0.005 au) and twice larger for M2 (0.011 au) shown in **Figures 5** and **6**, and specifically in **Figure 7** producing daily differences in the S-E distances for each month of the years for the two millennia considered. In the next two millennia this trend is expected to return back to the level in 600 and then in the next 4.2 thousand years to change to the opposite one, e.g. producing the Sun shift to the autumn equinox and the shifts of the local perihelion and aphelion for considered years towards early December and June, respectively, following the calculations by [30].

Interestingly, the annual variations of the S-E distances shown in **Figure 9** can explain the oscillations of the baseline solar magnetic field (Hallstatt's cycle) shown by dark blue lines in **Figure 3** and in **Figure 4** (top plot) [19] by the oscillation of the Earth aphelion and perihelion from the major axis. In M1 the Sun's location is closer to the ellipse focus of the Earth orbit resulting in a smaller magnitude of the Sun's shift in the direction of the minor axis that leads to the minimum of the baseline magnetic field of northern polarity, shown by the dark blue line in **Figure 3** (bottom plot) [19, 49]. While in M2 the Sun shifts much further from the focus towards the spring equinox position of the Earth orbit, so that there is a shift of the longest S-E distance (local aphelion) from 21 June (when the aphelion on the major axis of ellipse is approached) to 16 July when the aphelion is shifted from the major axis to the line of the ellipse connecting the ellipse centre and displacement of the Sun from the ellipse focus and directed under the angle  $\phi$  (see Eq. (1)) to the major axis.

Hence, in 1600–2600 the Earth will be turning closer to the Sun for up to 25 additional days after the summer solstice, while turned towards the Sun with its Northern hemisphere, before it approaches the local aphelion. This is likely to cause a small rise to the baseline magnetic field of northern polarity as shown in **Figure 3** (dark blue line) [19]. And given the periodic variations of the gravitational effects of four large planets described by [30], one can expect the similar periodic variations of the baseline magnetic field linked to the positions of the local aphelion and perihelion for a given epoch. Therefore, this confirms the hint expressed earlier [19, 49] that the baseline magnetic field oscillations derived there purely from the magnetic field observations are, indeed, caused by the gravitational effects of large planets on the Sun, or by solar inertial motion.

## 4. Millennial oscillations of solar irradiance with the sun-earth distances

### 4.1 Method of inverse squares

Following the variations of the S–E distances discussed in section 3, let us evaluate the variations of total solar irradiance (TSI) imposed by a change of these S-E distances in the millennia M1 and M2 using the method of inverse squares. A magnitude of the total solar irradiance  $S$  variations at the solar-Earth distance  $d$  by considering the Sun as a point body emitting radiation with an intensity  $I_{\odot}$  [50]:

$$S = \frac{I_{\odot}}{d^2}. \quad (2)$$

Hence, the solar irradiance  $S$  can vary either because of the variations of intensity  $I$  of solar radiation at the Sun itself or because of the variations of a distance  $d$



between the Sun and Earth. The variations of the solar intensity  $I$  is caused by the variations of solar activity induced by the electro-magnetic dynamo action in the solar interior.

If the intensity  $I_{\odot}$  of radiation on the Sun is considered to be constant at a given time ( $I_{\odot}=\text{const}$ ), then the solar irradiance  $S$  can also change because of a variation of the Sun-Earth distance caused by the Earth orbital motion itself leading to the terrestrial seasons and by solar inertial motion whose effects are not yet fully investigated. In any case, by knowing the ephemeris of the S-E distances and using Eq. (2) above for calculating solar irradiance at two different distances  $d_1$  and  $d_2$ , one can find the relationship between the solar irradiance,  $S_1$  and  $S_2$  at these distances, which follows the inverse square law [50]:

$$S_1 \cdot d_1^2 = S_2 \cdot d_2^2. \quad (3)$$

Therefore, if at a distance  $d_1$  the average solar irradiance is  $1366 \text{ W/m}^2$  [22, 31] then if the distance is changed to  $d_2$ , the solar irradiance  $S$  should also change following the Eq. (3). For example, if the distance  $d_2$  between the Earth and Sun was to be decreased by 0.016 au (as shown in section 3 for two millennia 600–2600) so that the initial irradiance of  $1366 \text{ W/m}^2$  divided by the square of the new distance results in the irradiance of  $1411 \text{ W/m}^2$ . The difference in the irradiance is  $1411-1366 = 45 \text{ W/m}^2$ , that is 3.3% that is exactly the magnitude mentioned in the first paragraph of the last section of paper [19].

In section below the solar irradiance is explored in more details for the two millennia from 600 to 2600 AD for the S-E distances presented in section 3.

#### 4.2 Orbital variations of solar irradiance in the millennia 600–2600

As established in section 3, the Sun-Earth distances are hanging accordingly to the ellipse curve as Kepler's 3rd law assigns. Instead, these distances are defined by the two motions: the Earth and Sun about the barycentre of the solar system with the latter caused by the gravitational effects of large planets of the solar system, or solar inertial motion (SIM). Therefore, the daily variations of solar irradiance over a year will be affected by the combination of the Earth revolution on its orbit and the Sun's revolution about the barycentre.

By using Eq. (3) let us calculate the solar irradiance at any day of a year during the two millennia M1 and M2. For the TSI normalisation the magnitude of  $S_1 = 1366 \text{ W/m}^2$  [31] can be used for the longest distance in June 1700. Then the daily TSI magnitudes for every month of a year for three years for each millennium: M1 (600, 1100, 1600) and M2 (1700, 2020, 2600) are presented in **Figure 11** (for January–June), and 12 (for July–December) with their annual variations compared in **Figure 13**. The small differences ( $\leq 0.001$  au) between the S-E distances of 1600 and 1700 are considered when calculating the total solar irradiance for M2. The overall variations of the sum of the TSI deposited to Earth in each year are presented in **Figure 14** calculated for: (a) the mean TSI magnitudes averaged for every month, e.g. by adding the TSI magnitudes for 12 months (left plot) and (b) the daily TSI magnitudes, e.g. by adding the TSI magnitudes for all days in each year considered.

In M1 the increase of solar irradiance during the months January–June is nearly balanced by its decrease from July to December (**Figures 11 and 12**, left column) while in M2 the solar irradiance is noticeably higher in February–July when the atmosphere is heated by the Sun than in July–December when the atmospheric cooling occurs (see **Figures 11 and 12**, right column). This is more evident in the

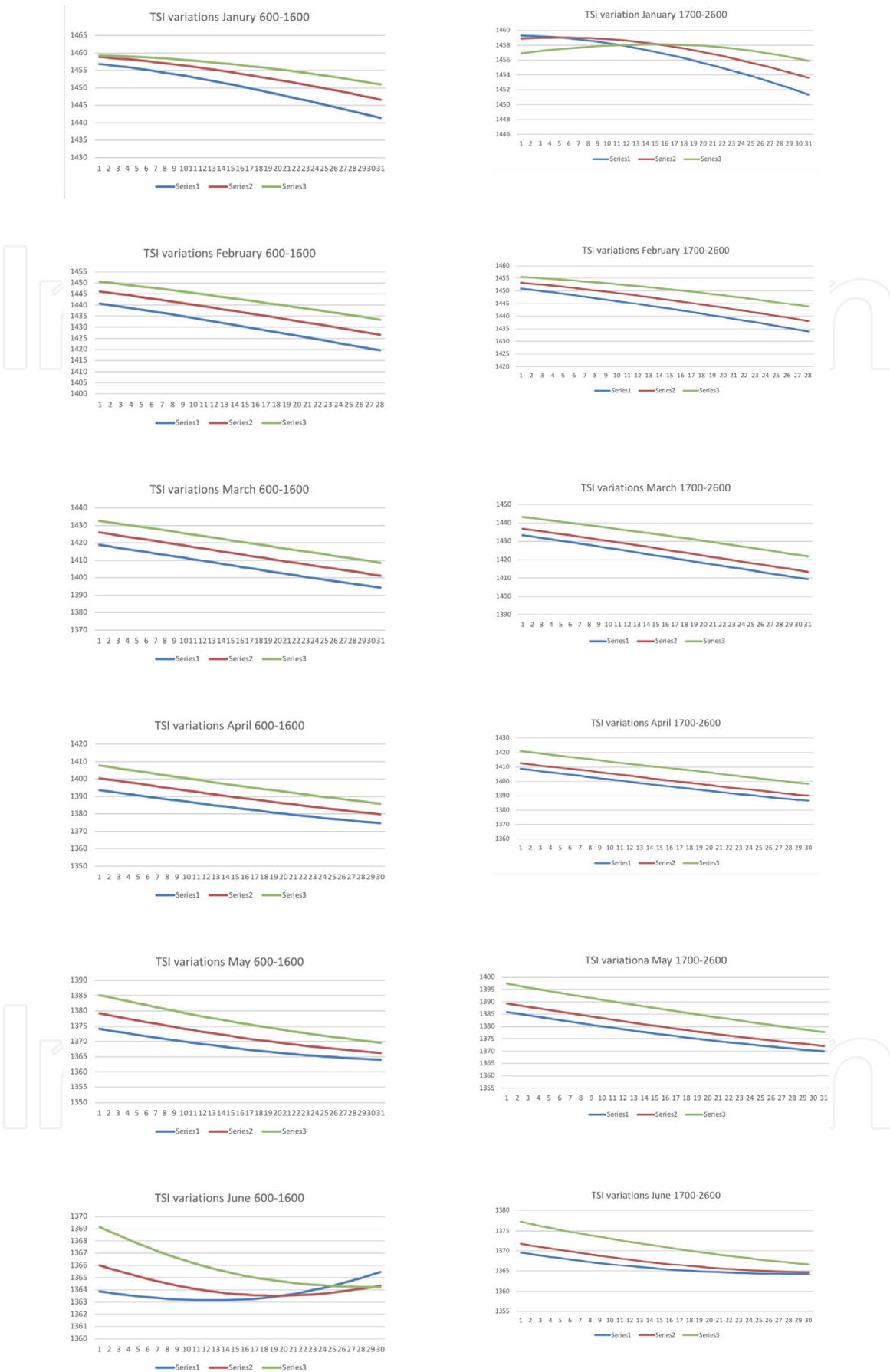


**Figure 11.** Variations of the daily solar irradiance in ( $W/m^2$ ) in January–June for three sample years selected in the millennia M1 (600–1600) (left) and M2 (1600–2600) (right). Left column: Blue - year 600, red -1100 and green -1600; right column: Blue - 1700, red - 2020 and grey - 2600. X-axis shows days of the months.

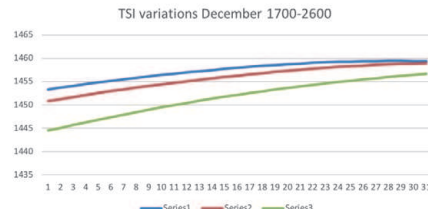
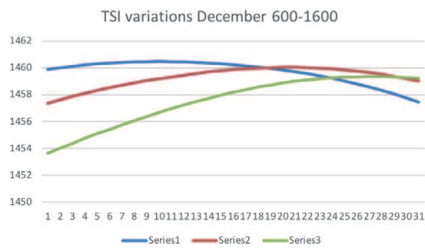
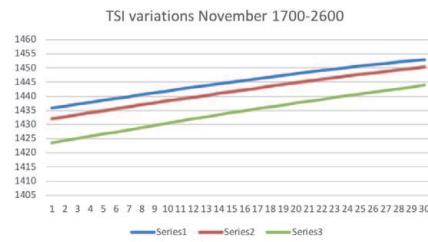
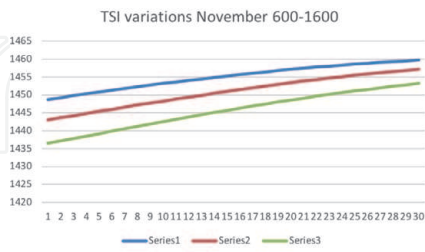
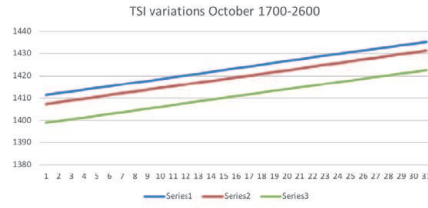
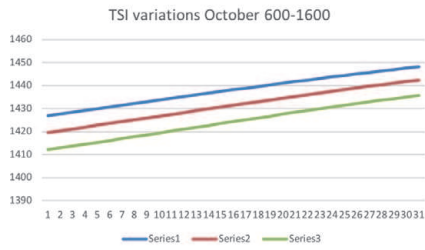
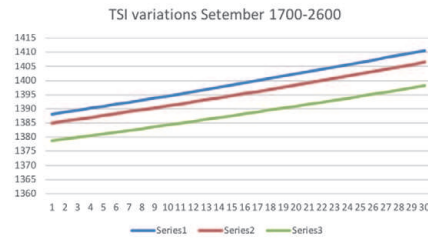
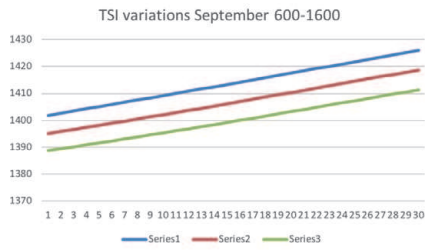
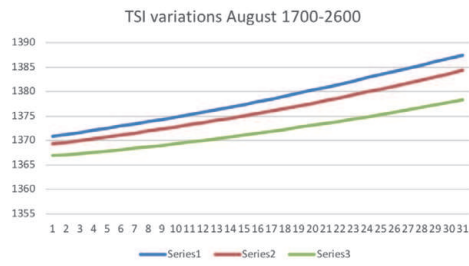
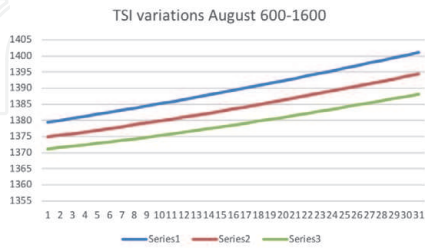
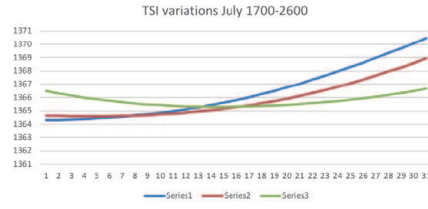
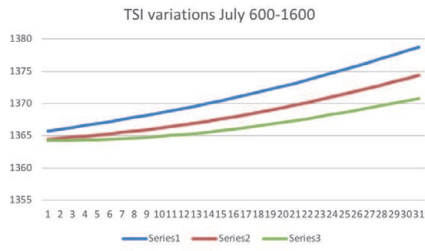


**Figure 12.** Variations of the daily solar irradiance ( $W/m^2$ ) in July–December of three sample years in the millennium M1 (600–1600) (left) and M2 (1600–2600) (right). Left column: Blue - 600, red - 1100 and green - 1600; right column: Blue - 1700, red - 2020 and grey - 2600. X-axis shows days of the months.

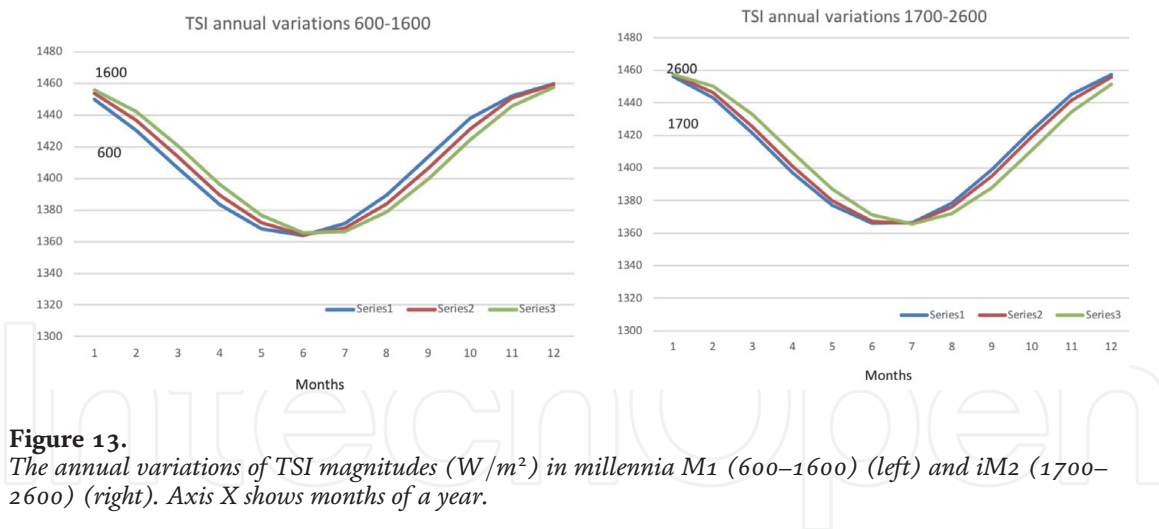


**Figure 13.** The annual variations of TSI magnitudes ( $W/m^2$ ) in millennia M1 (600–1600) (left) and iM2 (1700–2600) (right). Axis X shows months of a year.

annual variations of the monthly averaged TSI magnitudes (**Figure 13**) revealing a steady increase of the solar irradiance input in millennia M1 and, especially, in M2 during spring–summers and decrease during autumn–winters in the Northern hemisphere in each century caused by the variations of S–E distances shown in **Figure 9** discussed above.

Because of a reduction of the S–E distances in the first half of a year caused by SIM, the TSI deposition from years 1700 to 2600 is increased by about  $11 W/m^2$  (0.95%) in February–March (and decreased by the same amount in August–September), by  $15 W/m^2$  (1.2%) in April–May (decreased in October–November) and by  $7–8 W/m^2$  (0.5%) in June–July (decreased in December–January) (see **Figures 11** and **12**). These TSI variations can naturally explain a wide variety of the measured TSI magnitudes in the earlier space observations of  $1370 W/m^2$  (Shirley et al. 1990),  $1971 W/m^2$  (Wolff & Hickey 1987), or  $1972 W/m^2$  (Lee III et al. 1995) if they are measured during May–June or July–August. The numbers of TSI variations during a first half of a year can be added to produce more than 2.7% of solar irradiance increase in M2 because of the S–E distance decrease by SIM that is comparable with the estimations up to 3.5% hinted in the retracted paper [19]. *This amount* of the extra solar radiation input into the terrestrial atmosphere and ocean has not been yet considered in the current climate models.

The variations of solar irradiance averaged for every month in a year are plotted for both millennia in **Figure 13**, showing that the minimum of the mean solar irradiance is shifting in M2 towards 15 July, thus, securing the extra heating of Northern atmospheres in the summer months of second half of June and half of July in this millennium M2. These shifts of the largest S–E distances aphelion from 21 June to 15 July (local aphelion) in M2 can also explain why the baseline solar magnetic field is an ascending phase of Hallstatt’s current cycle, with a maximum of the northern polarity at 2600 before the longest distance becomes shifting back to June in the next few millennia. As shown in [19] (see **Figure 3**) there have been about 60 super-grand (Hallstatt’s) cycles over the past 120,000 year. This means such the millennial changes of the TSI on Earth are regular patterns, which will continue to appear in the current Hallstatt’s cycle shown in **Figure 4**, top plot [19].

Based on the location of Earth on its orbit, these solar irradiance inputs has to be divided between the hemispheres depending on which one of them is turned towards the Sun. This means that, because of the Earth axis tilt of  $23.5^\circ$  from the vertical to the ecliptics, in the millennium M1 (600–1600) the input of solar radiation in the Northern hemisphere was slowly increasing from January until 21 June not only because of the elliptic Earth orbit but also because of the Sun’s shift from the focus of this ellipse in the minor axis direction towards the spring equinox and



become reducing from 21 June through the whole July. While in M2 (1600–2600) during the months June – July the input of solar irradiance to the Northern hemisphere will be higher than in the elliptic orbit. This means that in M2 the increase of the solar input in February–July must be ahead of its decrease in August–January. This would happen also because, according to Kepler’s second law, the Earth moves slower at the parts of the orbit in June–July–August than in December–January, thus, passing quicker through the positions with a reduced radiation in December than with the increased one in June–July.

### 4.3 Imbalance of the TSI depositions in the two millennia

Since there is a shift of the minimum point of the TSI annual variations (**Figure 13**) from 21 June (M1) to 15 July (end of M2), this indicates a possible imbalance between the annual TSI input and output in M2 (1600–2600). From the daily magnitudes of TSI shown in **Figures 11** and **12**, it is possible to count the total annual amount of TSI emitted by the Sun towards the Earth in each year of the both millennia. If this amount does not change from year to year, then TSI is, indeed, the same for each year for both centuries, as currently assumed.

However, the real annual magnitudes of TSI deposited to the Earth during the two millennia are shown in **Figure 14** calculated for the two cases: (a) added together the averaged monthly TSI magnitudes (left plot) calculated for the S-E distances shown in **Figure 13** when only 12 magnitudes per year (for 12 months); (b) added together the daily TSI magnitudes (right plot) taken from **Figures 11** and **12** associated with the daily magnitudes of TSI (for 366 days for the leap years used).

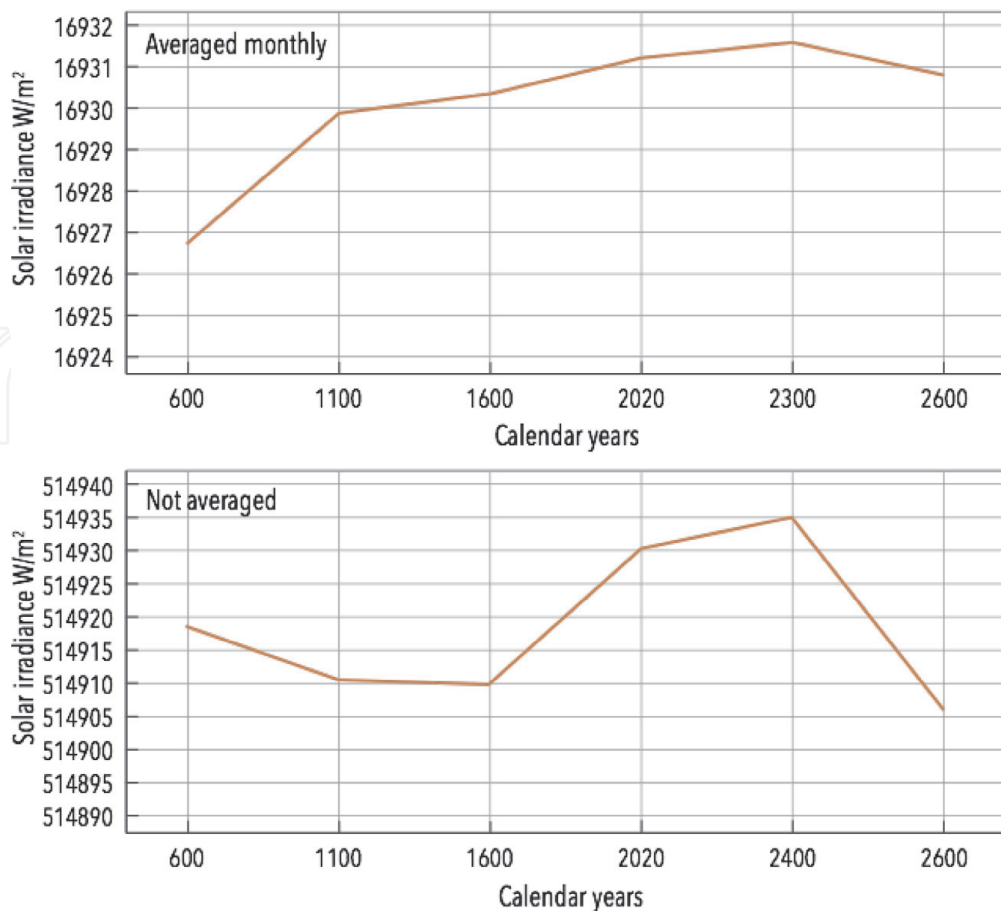


**Figure 14.** The total annual TSI variations ( $W/m^2$ ) in the millennia M1 and M2 derived by summation of the mean monthly (top) and daily TSI magnitudes (bottom). Axis X shows the years of the millennia.

These two plots clearly demonstrate that the monthly TSI variations (case a) show the increase of TSI by about  $1\text{--}1.3\text{ W/m}^2$  in 2020 compared to 1700 (**Figure 14**, left plot). This TSI increase found from the S-E distance ephemeris is close to the magnitude of  $1\text{--}1.5\text{ W/m}^2$  reported from the current TSI observations [34]. However, the annual TSI magnitudes, calculated from the daily S-E distances (case b) reveal a much larger annual increase of the total solar irradiance by about  $20\text{--}25\text{ W/m}^2$  ( $> 1.8\%$ ) in M2 (by 2500) than in millennium M1 (**Figure 14**, right plot). This analysis gives the indication of the averaged TSI increase in M2 could be  $2.5\text{--}2.8\text{ W/m}^2$  per century, or  $(0.18\text{--}0.20)\%$ , comparing to the TSI in 1700. This is the very important hidden solar irradiance input in millennium M2 (1600–2600) caused by the SIM effects, which was significantly underestimated if only the averaged monthly TSI magnitudes are used (**Figure 14**, compare left and right plots). The essential issue is how much of this extra solar radiation is distributed between the hemispheres owing to the Earth tilt, its position on the orbit or the level of exposure to solar radiation [42, 51].

Our study of the S-E distance variations shows that at the start of any year, in January, the Earth is turned to the Sun with its southern hemisphere, meaning that any decrease and increase of solar radiation during this time is mostly absorbed by the parts in Southern hemisphere. When the Earth's orbiting approaching March, the distribution of solar irradiance between the hemispheres becomes nearly even, while in April–June the main part of the solar radiation input is shifted towards the Northern hemisphere, having its maximum theoretically (by Kepler's law) on 21 June, while in reality, shifted to 5 July in 2020 and to 16 July in 2500. Hence, in M2 the Northern hemisphere should get the extra solar radiation not only in the first six months of a year but also in the 25 days from 21 June by approaching the local aphelion on 16 July, which is not compensated later by its expected cooling because of a shift of the local perihelion to 16 January.

By comparing the mean-by-time and mean-by-arc S-E distances for an elliptic orbit (see Appendices B and C) based on the calculated shifts of aphelion and perihelion [51] with the real S-E distances derived from the ephemeris one can conclude that the ephemeris of the S-E distances have to reflect the Sun shifts in SIM, in addition to the Earth revolution about the ellipse focus. Therefore, the solar radiation deposition in the millennium M2 is expected to be essentially higher than in millennium M1 and different from the standard seasonal changes because of the uneven shifts of Sun-Earth distances on the orbit owing to SIM. This extra TSI amount caused by SIM (from the variations of a distance  $d$  in formula (2)) will undoubtedly add to the magnitude of solar irradiance coming from the solar activity itself (or the parameter  $I_{\odot}$  in formula (2)) shown in **Figure 4** (bottom plot, blue lines) leading to the overall solar irradiance increase that, in turn, can account for a large amount of the terrestrial temperature increase shown by the red curves in **Figure 4** (bottom plot). This extra solar forcing caused by SIM needs to be taken into account in any climate models.

## 5. TSI variations and terrestrial temperature

Let us try to evaluate how these variations of solar irradiance can affect terrestrial temperature from the general similarity approach. The TSI variations caused by the solar activity in normal cycles of 11 years and during grand solar minima (similar to Maunder Minimum) can be described as follows.

1. Solar irradiance  $S$  variations at Earth owing to 11 year cycle is about 0.1% of the average magnitude of TSI  $S$  ( $1366\text{ Wm}^{-2}$  accepted in this study) increasing

by  $1.4 \text{ Wm}^{-2}$  during maxima and decreasing during minima [33, 54]. The terrestrial temperature variations during 11 year cycle are negligible.

2. Solar irradiance  $S$  variations at Earth owing to GSM is about  $2.5\text{--}3 \text{ W/m}^2$ , or 0.22 % of  $S$  [31, 39, 55] as shown in **Figure 2** (left plot). These estimations are also supported by conclusions by these authors [55, 56] showing sometimes up to 0.4% contributions of active regions into the solar radiance intensity  $I_{\odot}$ .

The terrestrial temperature curve presented in **Figure 2** (right plot) shown a reduction during MM of the average terrestrial temperature by about  $1^{\circ}\text{C}$  [36, 57, 58], e.g. the decrease of TSI by 0.11% secures a decrease of the terrestrial temperature by approximately  $0^{\circ}.5\text{C}$ . Let us use this simple estimation until we carry out more precise model simulations.

### 5.1 Expected effects of the TSI increase by SIM on the terrestrial temperature

The terrestrial temperature is found increasing since Maunder minimum as shown in **Figure 4**, bottom plot derived by Akasofu [35] that is close to the plot presented in the NASA and IPCC report <https://www.ipcc.ch/sr15/>. At the same time the solar activity of 11 years, and thus, solar irradiance in the past four solar cycles was decreasing.

Now we established that there is an additional effect leading to the increase of solar irradiance in the millennium M2 (1600–2600) because of the changing Sun-Earth distances imposed by the solar inertial motion (SIM) owing to gravitational effects from Jupiter, Saturn, Neptune and Uranus. The overall increase of solar irradiance for M2 is shown in **Figure 14** to reach about  $20\text{--}25 \text{ W/m}^2$  for the whole planet, which can be assumed to split evenly to each hemisphere with  $10\text{--}12 \text{ W/m}^2$ .

Although, the conversion of this extra solar radiation into the terrestrial temperature is a complex process involving exchanges between the deposited solar radiation to different hemispheres, ocean and atmospheric radiative transfer [59]. In fact, using line-by-line radiation transfer (LBL-RT) calculations under different cloudiness conditions, ground temperatures, and humidity models for radiative transfer of UV solar radiation by atmospheric molecules including  $\text{CO}_2$ , Hardy [59] has shown that even a smaller increase of solar radiation by  $5 \text{ W/m}^2$  leads to a noticeable (60%) increase of the terrestrial temperature defined by the Sun and only 40% defined by the  $\text{CO}_2$  emission. The further increase of solar irradiance owing to the millennial TSI misbalance derived here in section 4.3 from the ephemeris of the Sun-Earth distances would definitely lead to a further contribution (possibly, above 80%) of the Sun's radiation into the observed terrestrial temperature growth.

Although, in the current study we do not carry out radiative transfer simulations, and thus, can only roughly estimate possible variations of the average terrestrial temperature using the observed curves similar to those measured [35, 38] (**Figure 4**, bottom plot). The baseline temperature was shown to increase, or to recover from 'little ice age' after Maunder minimum, in the past three centuries (black straight line in [19, 35]). Since the TSI increase by up to  $25 \text{ W/m}^2$  for two hemispheres, or  $12.5 \text{ W/m}^2$  per hemisphere is expected until, at last, 2500, then using the link between the solar irradiance and terrestrial temperature derived from **Figure 2**, the increase in the baseline terrestrial temperature from 1700 can be expected by about  $4.0^{\circ}\text{C}$  in 2500, or by  $2.0^{\circ}\text{C}$  in 2100 and by  $1.5^{\circ}\text{C}$  in 2020.

However, these are rather rough estimations. Further investigation of the level of conversion of solar radiation into the atmospheric heating and radiation of

terrestrial atmosphere using radiative transfer simulations are required. This can provide more accurate numbers for the terrestrial temperature variations caused by the increase of solar irradiance owing to solar activity and SIM, in general, and their fluctuations in the hemispheres, in particular.

Note, this proposed prediction of the baseline temperature variations does not explain further temperature fluctuations above the baseline temperature which can well be caused by either anthropogenic or other terrestrial activities not considered on this paper.

## 5.2 Effects of upcoming grand solar minimum (2020–2053)

Although in the next 33 years the Sun is entering a period of the reduced solar activity, the modern grand solar minimum, which can be called a ‘mini ice age’, similar to Maunder Minimum. The GSMs are caused by significantly reduced solar magnetic field imposed by the disruptive interference of two magnetic waves generated by the double dynamo in the solar interior [10]. The first modern GSM1 occurs in 2020–2053 [10, 60] and the second modern GSM2 will happen in 2370–2415 [10, 60].

Because the solar irradiance and terrestrial temperature already increased since the MM owing to the SIM effects discussed in section 5.1, the terrestrial temperature during the first modern GSM1 is expected to drop by about 1.0°C to become just (1.5–1.0=) 0.5° C higher than that in 1700.

The temperature decrease during the second modern GSM (2375–2415) can be estimated calculated as follows. The current temperature increase in 2020 is by 1.5° C, which should increase by 2375 by another 1.5° C (=3 x 0.5C [35]) giving the total increase since 1700 by 3.0° C. The temperature decrease caused by a reduction of solar magnetic field and solar activity during the GSM2 would lead to a reduction of temperature by about 1.0° C. This will produce the total temperature during the GSM2 of (3.0–1.0=) 2.0°C higher than in 1700. After each of the modern GSMs, solar activity is expected to return to normal 11 year cycles as shown in **Figure 1** [10].

## 6. Conclusions

In this chapter the investigation of Sun-Earth distances from the ephemeris by VSOP87 [47] and JPL ephemeris [48] is presented. The Sun is found shifting in millennia M1 and M2 along the direction of the minor axis towards the spring equinox that leads to a significant reduction of S-E distances in January–June by about 0.005 au in M1 and up to 0.011 au in M2, which are followed by the asymmetric increases in the second half of the year (July–December). However, the S-E distance increases and decreases are not identical as expected from elliptic orbit.

These S-E distances are found affected not only by the Earth revolution about the focus of the ellipse, but also by the Sun’s motion about the barycentre caused by the gravitational effects of other planets (Jupiter, Saturn, Neptune and Uranus), or solar inertial motion (SIM). This shift of the position of the Sun with respect to the barycentre has been recognised as the solar inertial motion - SIM [25, 27, 30]. The resulting S-E distances are defined by the superposition of these two motion: Earth revolution and SIM. The similar inertial motion effects are often observed in other stars, which have planetary systems, leading to the wobbling star effect that is used to trace possible exoplanets [52, 53].



The S-E distance shifts are found to lead to a migration of the Earth's aphelion and perihelion from its classic positions on the major axis of the ellipse to occur on 21 June and 21 December, respectively, appropriate for the ideal elliptic Earth revolution. For example, the aphelion is shifted: in 1600 to 28 June, in 2020 to 5 July and in 2060 to 16 July, while and the perihelion migrates from 21 December to 28 December in 1600, 5 January in 2020 and to 16 January in 2600. The shifts of the S-E distances lead to the shifts of the Earth aphelion and perihelion from the major ellipse axis to the intermediate (shorter) axis, which passes through the SIM position of the Sun for the year and the ellipse orbit centre. Therefore, these shifts define the skewness of Sun-Earth distances along the Earth orbit towards the real position of the Sun, because it is moved outside the focus owing to the orbital perturbations of the Sun's motion about the barycentre caused by the gravitational forces of the four large planets.

These shifts of Sun-Earth distances lead to the changes in the total solar irradiance reaching the Earth atmosphere and baseline magnetic field measured from the Earth. Because of this reduction of the S-E distances caused by SIM, the TSI at the Earth is shown to increase from 1700 to 2600 by about  $11 \text{ W/m}^2$  (0.95%) in February–March (and decreased in August–September), by  $15\text{--}18 \text{ W/m}^2$  (1.2%) in April–May (and decrease in October–November) and by  $7\text{--}8 \text{ W/m}^2$  (0.5%) in June–July (and decrease in December–January). While the shift of the maximal distance (aphelion) from regular 21 June date in 1600 to mid-July in 2600 can naturally explain the skewness of the baseline magnetic field towards the Northern polarity in 2600 and the minimum of the baseline magnetic field in 1600, by its skewness towards Southern polarity as it was reported before [19, 49].

It is also shown that since 1600 to 2020 there was an increase of the annual TSI magnitude by about  $1.3 \text{ W/m}^2$  derived from the mean monthly S-E distances, which is close to the magnitude of  $1\text{--}1.5 \text{ W/m}^2$  reported for the similar period from the current TSI observations [34]. However, the annual TSI magnitudes, calculated from the daily S-E distances reveal a much larger annual increase of the total solar irradiance by about  $20\text{--}25 \text{ W/m}^2$  by 2500 in M2 compared to millennium M1. This means there is an excess of solar radiation input into the terrestrial atmosphere in millennium M2 not accounted for by any other consideration that has to be considered for the solar forcing. This additional solar input should have different redistribution between Northern and Southern hemispheres in addition to normal variations of the Earth position on elliptic orbit [51] linked to their exposure time to the solar input not discussed in the current paper.

However, in 2020 the Sun has entered the period of a reduced solar activity: the Grand Solar Minimum (2020–2053). The orbital variations of solar irradiance will be combined with variations of solar activity, or solar magnetic field, imposed by the variations of solar dynamo [1, 10]. The decrease of solar irradiance during this GSM is expected to be about  $3 \text{ W/m}^2$ , or 0.22%. Therefore, the reduction of solar irradiance caused by the GSM effect will work in opposition to the increase of solar irradiance caused by the orbital SIM effects in the current Hallstatt's cycle.

The baseline temperature (not including any terrestrial effects) is shown increased by 2020 by  $1.5^\circ\text{C}$  since 1700 because of SIM effects. Because of the modern GSM1 the terrestrial temperature is expected to be lowered by  $1.0^\circ\text{C}$  giving the resulting temperature of  $0.5^\circ\text{C}$  higher than it was in 1700. After 2053, the solar irradiance and the baseline terrestrial temperature is expected to return to the pre-GSM level. Then the irradiance and temperature will continue increasing because of the SIM effects combined with radiative transfer of solar radiation in the terrestrial atmosphere. This means the terrestrial temperature will continue increasing up to  $3.0^\circ\text{C}$  by 2375 when the second modern GSM2 will occur (2375–2415). During GSM2

the temperature is to be reduced again by 1.0°C to reaching the magnitudes of 2.0°C higher than it was in 1700.

Therefore, our analysis with the new proxy of solar activity (SBMF) has opened new perspectives for reliable prediction of solar activity on short, medium and long-terms. This approach has allowed us to link the solar magnetic field variations to the variations of solar irradiance, which are associated with both the inner solar processes and the orbital effects on the Sun-Earth distances. The fundamental oscillations of solar irradiance, in turn, can be linked to the oscillations of the baseline terrestrial temperature, independent of any terrestrial processes of radiative transfer and heating. Although, other terrestrial and anthropogenic effects can lead to the fluctuations of this temperature but their study was outside the scope of the current chapter.

## Acknowledgements

V. Zharkova wishes to express her deepest gratitude to the funding by the public supporters raised through ‘Fund-me’ sites. Their support inspired the author to undertake the investigation of the ephemeris of the Sun-Earth distances and relevant variations of the solar irradiance associated with the changes of the Sun-Earth distances induced by orbital effects. The author also wishes to thank the Paris Observatory, France and JPL ephemeris websites, JPL, Pasadena, US for providing the ephemeris of the Sun-Earth distances for a few millennia. The work was partially supported by the US Airforce grant PRJ02156.

## Appendix

### A. Basics of planetary orbits.

In order to investigate the orbital effects on the distance between the Sun and Earth and the resulting variations of solar irradiance imposed by these variations, let us first remind the basic laws governing the planet revolution about a central star, the Sun. It is suggested that the planets evolution about the central star (Sun) is defined by Kepler’s three laws [61]:

1. Planets move in elliptical orbits around the central star (Sun), which is located in one of the foci of the ellipse (see **Figure 15**, left plot).
2. The Sun-planet line sweeps out equal areas in the equal times. This means that planets move faster when they are nearer the Sun (perihelion) and slower when they are further away (aphelion).
3. The square of the orbital period of a planet is directly proportional to the cube of the semi-major axis  $a$  of its orbit. This law defines the Sun-Earth distances at any point of the orbit.

The Sun is located in one of the two foci (point -C in **Figure 15**) of the ellipse with a semi-major axis  $a$  and a semi-minor axis  $b$  and the eccentricity:

$$e = \sqrt{1 - \frac{b^2}{a^2}}, \quad (4)$$

It can be noted that is a link between the semi-major and semi-minor axis:

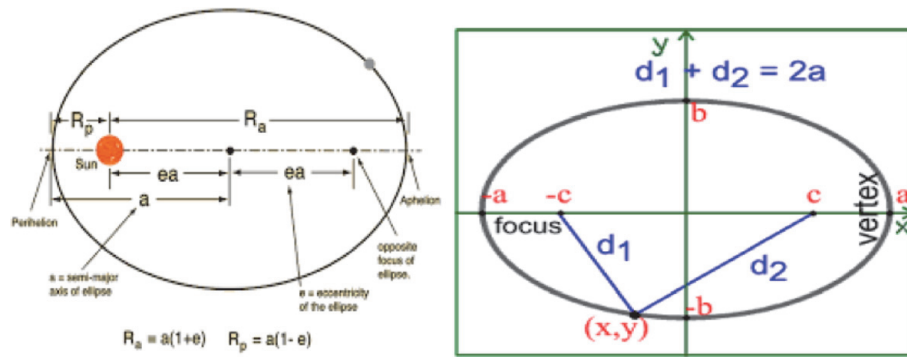


**Figure 15.** Elliptic orbit of the earth revolution about the sun located in the left focus of the ellipse with a semi-major axis  $a$ , a semi-minor axis  $b$  and the eccentricity  $e$ .

$$b^2 = a^2(1 - e^2). \quad (5)$$

The planet is located in the point  $(x,y)$  on the orbit on a distance  $d$  from the focus C under the angle  $\theta$  to the major axis (see **Figure 15**, right plot).

This distance  $d$  is defined by Kepler's third law as follows:

$$d = \frac{a(1 - e^2)}{1 - e \cos \theta}, \quad (6)$$

where  $0 \leq e \leq 1$ .

Let us introduce  $R_a$  the aphelion distance from the focus where the star is located, to the longest point of the orbit along the major axis and  $R_p$  - the perihelion distance from the focus to the closest point along the major axis. Using this Eq. (6) one can calculate the aphelion  $R_a$  and perihelion  $R_p$  distances by setting the angle  $\theta$  equal to zero for aphelion and  $180^\circ$  for perihelion, e.g.

$$R_a = a(1 + e), \quad (7)$$

$$R_p = a(1 - e). \quad (8)$$

The sum of the distances  $d_1$  and  $d_2$  from a planet location on the orbit to the both foci of the ellipse is constant and equal  $2a$ , e.g.

$$d_1 + d_2 = 2a = R_a + R_p. \quad (9)$$

where  $d_1$  and  $d_2$  are distances from the two foci to the current position of a planet (see **Figure 15**, left plot).

## B. Average distances of a planet from the focus of ellipse

There are three average distances of a planet from the star can be calculated averaged in: (a) the angle  $\theta$ ; (b) time; and (c) arc length  $s$  [62]. The formula (6) for the planet distance from the ellipse focus, according to Kepler's third law, can be rewritten as follows:

$$d = \frac{P_e}{1 - e \cos \theta}. \quad (10)$$

where  $P_e = a(1 - e^2)$ .

## B.1 Planet distance averaged in angle

Average distance  $\bar{d}_\theta$  in angle  $\theta$  is defined by the integral:

$$\bar{d}_\theta = \frac{1}{2\pi} \int_0^{2\pi} d \cdot d\theta = \frac{1}{2\pi} \int_0^{2\pi} \frac{P_e}{1 - e \cos \theta} d\theta = \frac{2\pi P_e}{2\pi \sqrt{\left(1 - e^2 = \frac{a(1-e^2)}{\sqrt{1-e^2}}\right)}} \quad (11)$$

so that

$$\bar{d}_\theta = a\sqrt{1 - e^2} = b, \quad (12)$$

Hence, the average distance by  $\theta$  is equal to the semi-minor axis  $b$ .

## B.2 Planet distance averaged in time

Average in time distance  $\bar{d}_t$  is defined by the integral for the period of a planet revolution  $T$ :

$$\bar{d}_t = \frac{1}{T} \int_0^T d dt, \quad (13)$$

Since according to the second Kepler's law, the radial arm of a given planet sweeps out an area at a constant rate  $h$ :

$$h = \frac{1}{2} d^2 d\theta / dt, \quad (14)$$

or

$$dt/d\theta = d^2 / 2h. \quad (15)$$

We know that the area of the ellipse is  $Th = \pi ab$ . Hence, the average distance in time can be defined as:

$$\bar{d}_t = \frac{1}{T} \int_0^T d \cdot dt = \frac{h}{\pi ab} \int_0^{2\pi} d \cdot (dt/d\theta) d\theta = \frac{h}{\pi ab} \int_0^{2\pi} d \frac{d^2}{2h} d\theta = \frac{1}{2\pi ab} \int_0^{2\pi} d^3 d\theta, \quad (16)$$

where

$$\frac{1}{2\pi ab} \int_0^{2\pi} d^3 d\theta = \frac{p^3 e^3 (2 + e^2) \pi}{1 - e^2)^{(5/2)} = b(3a^2 - b^2) \pi. \quad (17)$$

Then the average in time distance is

$$\bar{d}_t = \frac{1}{T} \int_0^T d dt = \frac{b(3a^2 - b^2) \pi}{2\pi ab} = 3a/2 - b^2/2a = \frac{3a}{2} - \frac{a^2(1 - e^2)}{2a} = a \left(1 + \frac{e^2}{2}\right). \quad (18)$$

or the averaged by time distance is



$$\bar{d}_t = a \left( 1 + \frac{e^2}{2} \right), \quad (19)$$

which is larger than the semi-major axis  $a$  by a factor of  $(1 + e^2/2)$ .

### B.3 Average distance in arc length

The integral for the arc length of an ellipse cannot be evaluated in finite terms, we need to proceed indirectly utilising the defining property of an ellipse that the sum of the distances from any point of the ellipse for the two foci is constant as described by Eq. (9). Let  $L$  to be the whole length of the orbit.

From the point of symmetry:

$$\int_0^L d_1 ds = \int_0^L d_2 ds. \quad (20)$$

Since by the definition of the ellipse  $d_1 + d_2 = 2a$  (see Eq. (9)), hence:

$$\int_0^L (d_1 + d_2) ds = 2aL, \text{ or} \quad (21)$$

$$\int_0^L d \cdot ds = aL. \quad (22)$$

Then the distance  $r_s$  averaged by the arc length is given by the expression:

$$\bar{d}_s = \frac{1}{L} \int_0^L d \cdot ds = aL/L = a. \quad (23)$$

Therefore, for the ideal revolution of a planet in ellipse about the star located in the ellipse focus, the average distance of the planet from the focus is defined by the parameters of the ellipse, along which the planet moves about the assumed location of the star if there are no other gravitational effects are considered.

### C. Average distances versus aphelion/perihelion variations.

The first step in investigation of millennial variations of solar irradiance and baseline magnetic field came from a suggestion of changing Sun-Earth distances because of a change of the Earth orbit shape. In fact, the ephemeris show [48] that since 1600 the Earth orbit's aphelion is found steadily decreasing while its perihelion is increasing (see **Figure 16**). Could this change of the Earth orbit cause the millennial changes of solar irradiance and magnetic field baseline? Let us explore this option. Sun is located in the ellipse focus, the S-E distance variations are affected by the variations of the Earth orbit parameters: aphelion and perihelion distances which are calculated by JPL. The link between the semi-minor axis  $b$  and the semi semi-major axis  $a$  can be written as follows:

$$2b = \sqrt{(d_1 + d_2)^2 - f^2}; \quad (24)$$

where  $d_1$  and  $d_2$  are the distances from the two ellipse foci to any point on the orbit,  $f$  is the distance between the foci of the ellipse, e.g.  $f = R_a - R_p$ . For

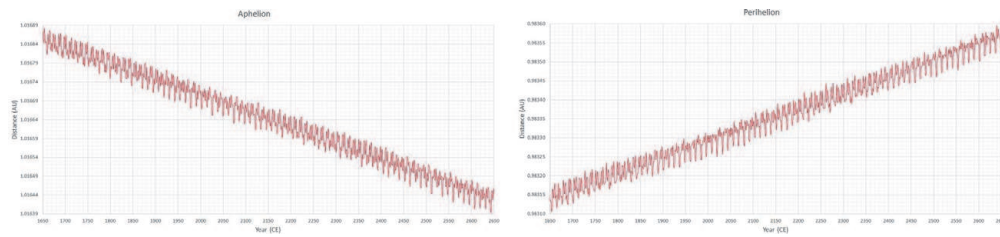


**Figure 16.** Variations of the aphelion (left) and perihelion (right) distances of the Earth orbit in the millennium M2.

calculation of  $d_1 + d_2$  we use the Eq. (9) that provides the relations for the semi-major  $a$  and the semi-minor  $b$  distances via the aphelion  $R_a$  and perihelion  $R_p$  as follows:

$$2b = \sqrt{(d_1 + d_2)^2 - f^2} = 2\sqrt{R_a R_p} \quad (25)$$

$$a = \frac{R_a + R_p}{2}. \quad (26)$$

Hence, if we fix for some time  $t_0$  the aphelion  $R_{a0}$  and perihelion  $R_{p0}$  distances, and assume that they are proportionally changed after some time by a magnitude  $\Delta$ , so that  $R_a = R_{a0} - \Delta$  and  $R_p = R_{p0} + \Delta$ , so that  $R_a + R_p = R_{a0} + R_{p0}$  and  $f = R_{a0} - R_{p0} - 2\Delta$ . Then from Eq. (24) the semi-minor axis can be calculated as follows:

$$\begin{aligned} 2b &= \sqrt{(d_1 + d_2)^2 - f^2} = \sqrt{(R_{a0} + R_{p0})^2 - (R_{a0} - R_{p0} - 2\Delta)^2} = \\ &= \sqrt{4R_{a0}R_{p0} + 4\Delta[R_{a0} - R_{p0} - \Delta]}. \end{aligned} \quad (27)$$

Giving the relationships between the the ellipse axes  $a$  and  $b$  and aphelion and perihelion distances.

$$a = R_a + R_b = R_{a0} + R_{p0}; \quad (28)$$

$$b = \sqrt{R_{a0}R_{p0} + \Delta[R_{a0} - R_{p0} - \Delta]}. \quad (29)$$

It is evident from the equations above that variations of the aphelion and perihelion distances will affect only the Earth semi-minor axis  $b$  and, thus, eccentricity  $e$ . Let us use them for estimation of the Earth orbit parameters from the ephemeris of aphelion and perihelion presented in **Figure 16**.

In the case of decreasing aphelion and increasing perihelion distances for a elliptic orbit with the star in its focus shown in **Figure 16**, it occurs from Eq. (29) that  $b$  will increase, while the orbit eccentricity  $e$  would decrease. By comparing the variations of the Earth aphelion and perihelion distances in 1500–2500 we evaluated the following changes. The variations of the aphelion and perihelion distances produce the reduction of eccentricity from 0.0170 in 1500 to 0.0163 in 2500. This would lead to a change of the average-by-time Sun-Earth distance from 1.0001462 au in 1600 to 1.0001328 au in 2500, e.g. the difference is virtually negligible and cannot be reflected in a noticeable change of solar irradiance. This indicates that over the whole millennium 1600–2600 the Earth orbit remains, in fact, a pretty stable elliptic orbit. However, the average S-E distances in this elliptic orbit do not change to such the extent to produce noticeable variations of solar irradiance or magnetic field baseline.

IntechOpen

IntechOpen

### **Author details**

Valentina Zharkova

Department of Mathematics, Physics and Electrical Engineering, Faculty of Engineering and Environment, Northumbria University , Newcastle Upon Tyne, United Kingdom

\*Address all correspondence to: [valja46@googlemail.com](mailto:valja46@googlemail.com)

### **IntechOpen**

---

© 2021 The Author(s). Licensee IntechOpen. This chapter is distributed under the terms of the Creative Commons Attribution License (<http://creativecommons.org/licenses/by/3.0>), which permits unrestricted use, distribution, and reproduction in any medium, provided the original work is properly cited. 

## References

- [1] E. N. Parker. Hydromagnetic Dynamo Models. *Astrophysical Journal*, 122:293, September 1955.
- [2] Rudolf Wolf. Studies on the frequency of Sun-spots, and on their connexion with the Magnetic Declination-variation. *Mon. Not. of the Royal Astron. Soc.*, 30:157, April 1870.
- [3] W. Maunder, Mrs. Wolfer's relative sun-spot numbers. *Mon. Not. of the Royal Astron. Soc.*, 64:226–+, January 1904.
- [4] H. W. Babcock. The Topology of the Sun's Magnetic Field and the 22-YEAR Cycle. *Astrophysical Journal*, 133:572, March 1961.
- [5] M. Stix. Differential rotation and the solar dynamo. *Astronomy and Astrophysics*, 47:243–254, March 1976.
- [6] S. Zharkov, E. Gavryuseva, and V. Zharkova. The Observed Long- and Short-Term Phase Relation between the Toroidal and Poloidal Magnetic Fields in Cycle 23. *Solar Physics*, 248:339–358, April 2008.
- [7] V. V. Zharkova, S. J. Shepherd, and S. I. Zharkov. Principal component analysis of background and sunspot magnetic field variations during solar cycles 21–23. *Mon. Not. of the Royal Astron. Soc.*, 424:2943–2953, August 2012.
- [8] V. Zharkova, E. Popova, S. Shepherd, and S. Zharkov. Reply to comment on the paper “on a role of quadruple component of magnetic field in defining solar activity in grand cycles” by Usoskin (2017). *Journal of Atmospheric and Solar-Terrestrial Physics*, 2018.
- [9] S. J. Shepherd, S. I. Zharkov, and V. V. Zharkova. Prediction of Solar Activity from Solar Background Magnetic Field Variations in Cycles 21–23. *Astrophysical Journal*, 795:46, November 2014.
- [10] V. V. Zharkova, S. J. Shepherd, E. Popova, and S. I. Zharkov. Heartbeat of the Sun from Principal Component Analysis and prediction of solar activity on a millennium timescale. *Nature Scientific Reports*, 5:15689, October 2015.
- [11] E. Popova, V. Zharkova, and S. Zharkov. Probing latitudinal variations of the solar magnetic field in cycles 21–23 by Parker's Two-Layer Dynamo Model with meridional circulation. *Annales Geophysicae*, 31:2023–2038, November 2013.
- [12] J. Zhao, R. S. Bogart, A. G. Kosovichev, T. L. Duvall, Jr., and T. Hartlep. Detection of Equatorward Meridional Flow and Evidence of Double-cell Meridional Circulation inside the Sun. *Astrophysical Journal Letters*, 774:L29, September 2013.
- [13] S. Zharkov, V. V. Zharkova, and S. S. Ipson. Statistical Properties Of Sunspots In 1996 2004: I. Detection, North South Asymmetry And Area Distribution. *Solar Physics*, 228:377–397, May 2005.
- [14] B. Belucz and M. Dikpati. Role of Asymmetric Meridional Circulation in Producing North-South Asymmetry in a Solar Cycle Dynamo Model. *Astrophysical Journal*, 779:4, December 2013.
- [15] J. Shetye, D. Tripathi, and M. Dikpati. Observations and Modeling of North-South Asymmetries Using a Flux Transport Dynamo. *Astrophysical Journal*, 799:220, February 2015.
- [16] J. A. Eddy. The Maunder Minimum. *Science*, 192:1189–1202, June 1976.
- [17] V. V. Zharkova, S. J. Shepherd, E. Popova, and S. I. Zharkov. Reinforcing a



Double Dynamo Model with Solar-Terrestrial Activity in the Past Three Millennia. In *Space Weather of the Heliosphere: Processes and Forecasts*, 2018.

[18] S. K. Solanki, I. G. Usoskin, B. Kromer, M. Schüssler, and J. Beer. Unusual activity of the Sun during recent decades compared to the previous 11,000 years. *Nature*, 431:1084–1087, October 2004.

[19] V. V. Zharkova, S. J. Shepherd, S. I. Zharkov, and E. Popova. RETRACTED ARTICLE: Oscillations of the baseline of solar magnetic field and solar irradiance on a millennial timescale. *Scientific Reports*, 9:9197, June 2019.

[20] L. E. A. Vieira, S. K. Solanki, N. A. Krivova, and I. Usoskin. Evolution of the solar irradiance during the Holocene. *Astronomy and Astrophysics*, 531:A6, July 2011.

[21] F. Steinhilber, J. Beer, and C. Fröhlich. Total solar irradiance during the Holocene. *Geophysics Research Letters*, 36(19):L19704, October 2009.

[22] F. Steinhilber, J. A. Abreu, J. Beer, I. Brunner, M. Christl, H. Fischer, U. Heikkila, P. W. Kubik, M. Mann, K. G. McCracken, H. Miller, H. Miyahara, H. Oerter, and F. Wilhelms. 9,400 years of cosmic radiation and solar activity from ice cores and tree rings. *Proceedings of the National Academy of Science*, 109(16):5967–5971, April 2012.

[23] Paul D. Jose. Sun's motion and sunspots. *Astronomical journal*, 70:193, April 1965.

[24] R. W. Fairbridge and J. H. Shirley. Prolonged minima and the 179-yr cycle of the solar inertial motion. *Solar Physics*, 110:191–210, March 1987.

[25] I. Charvatova. The solar motion and the variability of solar activity.

*Advances in Space Research*, 8(7):147–150, January 1988.

[26] James H. Shirley, Kenneth R. Sperber, and Rhodes W. Fairbridge. Sun's Inertial Motion and Luminosity. *Solar Physics*, 127(2):379–392, June 1990.

[27] Milan Paluš, Jürgen Kurths, Udo Schwarz, Norbert Seehafer, Dagmar Novotná, and Ivanka Charvátová. The solar activity cycle is weakly synchronized with the solar inertial motion. *Physics Letters A*, 365(5–6):421–428, June 2007.

[28] R. Mackey. Rhodes Fairbridge and the idea that the solar system regulates the Earth's climate. *Journal of Coastal Research*, (Proceedings of the Ninth International Coastal Symposium, Gold Coast, Australia), 51, May 2007.

[29] I. Charvátová. Can origin of the 2400-year cycle of solar activity be caused by solar inertial motion? *Annales Geophysicae*, 18(4):399–405, April 2000.

[30] A. S. Perminov and E. D. Kuznetsov. Orbital Evolution of the Sun-Jupiter-Saturn-Uranus-Neptune Four-Planet System on Long-Time Scales. *Solar System Research*, 52(3):241–259, May 2018.

[31] Judith Lean, Juerg Beer, and Raymond Bradley. Reconstruction of solar irradiance since 1610: Implications for climate change. *Geophysics Research Letters*, 22(23):3195–3198, January 1995.

[32] Charles L. Wolff and John R. Hickey. Solar Irradiance Change and Special Longitudes Due to  $\gamma$ -Modes. *Science*, 235(4796):1631–1633, March 1987.

[33] III Lee, Robert B., M. Alan Gibson, Robert S. Wilson, and Susan Thomas. Long-term total solar irradiance

variability during sunspot cycle 22. *Journal of Geophysics Research*, 100 (A2):1667–1676, February 1995.

[34] N. A. Krivova, S. K. Solanki, and Y. C. Unruh. Towards a long-term record of solar total and spectral irradiance. *Journal of Atmospheric and Solar-Terrestrial Physics*, 73(2–3):223–234, February 2011.

[35] S.-I. Akasofu. On the recovery from the little ice age. *Natural Science*, 2: 1211–1224, November 2010.

[36] D. J. Easterbrook. *Evidence-based Climate Science*. Elsevier, May 2016.

[37] P.J. *et al* Reimer. INTCAL09 AND MARINE09 RADIOCARBON AGE CALIBRATION CURVES 0–50,000 YEARS CAL BP. *Radiocarbon*, 51:1111–1150, 2009.

[38] P. Stauning. Solar activity-climate relations: A different approach. *Journal of Atmospheric and Solar-Terrestrial Physics*, 73(13):1999–2012, August 2011.

[39] Judith Lean. Evolution of the Sun's Spectral Irradiance Since the Maunder Minimum. *Geophysics Research Letters*, 27(16):2425–2428, August 2000.

[40] Y. M. Wang, J. L. Lean, and Jr. Sheeley, N. R. Modeling the Sun's Magnetic Field and Irradiance since 1713. *Astrophysical Journal*, 625(1):522–538, May 2005.

[41] J. D. Hays, John Imbrie, and N. J. Shackleton. Variations in the Earth's Orbit: Pacemaker of the Ice Ages. *Science*, 194(4270):1121–1132, December 1976.

[42] M. Milankovich. Canon of Insolation and the Ice Age Problem. *Zavodza Udzbenike i Nastavna Sredstva*, pages 307–310, April 1998.

[43] L. E. A. Vieira, S. K. Solanki, N. A. Krivova, and I. Usoskin. *VizieR Online*

*Data Catalog: Evolution of solar irradiance during Holocene* (Vieira+, 2011). *VizieR Online Data Catalog*, pages J/A+A/531/A6, May 2011.

[44] I. G. Usoskin, Y. Gallet, F. Lopes, G. A. Kovaltsov, and G. Hulot. Solar activity during the Holocene: the Hallstatt cycle and its consequence for grand minima and maxima. *Astronomy and Astrophysics*, 587:A150, March 2016.

[45] N. Scafetta. Discussion on the spectral coherence between planetary, solar and climate oscillations: a reply to some critiques. *Astrophysics and Space Science*, 354:275–299, December 2014.

[46] Rodolfo G. Cionco and Dmitry A. Pavlov. Solar barycentric dynamics from a new solar-planetary ephemeris. *Astronomy and Astrophysics*, 615:A153, July 2018.

[47] P. Bretagnon and G. Francou. Planetary Theories in rectangular and spherical variables: VSOP87 solution. *Astronomy and Astrophysics*, 202:309, August 1988.

[48] W. M. Folkner, J. G. Williams, D. H. Boggs, R. S. Park, and P. Kuchynka. The Planetary and Lunar Ephemerides DE430 and DE431. *Interplanetary Network Progress Report*, 42-196:1–81, February 2014.

[49] V. V. Zharkova, S. J. Shepherd, and E. Popova. Oscillations of the baseline of solar magnetic field and solar irradiance on a millennial timescale. *arXiv e-prints*, page arXiv:2002.06550, February 2020.

[50] D. Halliday, R. Resnick, and J. Walker. *Fundamentals of Physics: Extended*. Wiley, Germany, 2010.

[51] Duncan Steel. Perihelion precession, polar ice and global warming. *Journal of Cosmology*, 22:10106–10129, March 2013.

- [52] V. S. Airapetian, R. Barnes, O. Cohen, G. A. Collinson, W. C. Danchi, C. F. Dong, A. D. Del Genio, K. France, K. Garcia-Sage, A. Gloer, N. Gopalswamy, J. L. Grenfell, G. Gronoff, M. Güdel, K. Herbst, W. G. Henning, C. H. Jackman, M. Jin, C. P. Johnstone, L. Kaltenegger, C. D. Kay, K. Kobayashi, W. Kuang, G. Li, B. J. Lynch, T. Lüftinger, J. G. Luhmann, H. Maehara, M. G. Mlynczak, Y. Notsu, R. A. Osten, R. M. Ramirez, S. Rugheimer, M. Scheucher, J. E. Schlieder, K. Shibata, C. Sousa-Silva, V. Stamenković, R. J. Strangeway, A. V. Usmanov, P. Vergados, O. P. Verkhoglyadova, A. A. Vidotto, M. Voytek, M. J. Way, G. P. Zank, and Y. Yamashiki. Impact of space weather on climate and habitability of terrestrial-type exoplanets. *International Journal of Astrobiology*, 19(2):136–194, April 2020.
- [53] Kevin France. Exploring extreme exoplanets. *Nature Astronomy*, 4:1112–1112, November 2020.
- [54] Richard C. Willson and Hugh S. Hudson. The Sun’s luminosity over a complete solar cycle. *Nature*, 351(6321): 42–44, May 1991.
- [55] M. Fligge and S. K. Solanki. The solar spectral irradiance since 1700. *Geophysics Research Letters*, 27(14): 2157–2160, August 2000.
- [56] M. Lockwood and R. Stamper. Long-term drift of the coronal source magnetic flux and the total solar irradiance. *Geophysics Research Letters*, 26(16):2461–2464, January 1999.
- [57] Drew T. Shindell, Gavin A. Schmidt, Michael E. Mann, David Rind, and Anne Waple. Solar Forcing of Regional Climate Change During the Maunder Minimum. *Science*, 294(5549):2149–2152, December 2001.
- [58] Gifford H. Miller, Áslaug Geirsdóttir, Yafang Zhong, Darren J. Larsen, Bette L. Otto-Bliesner, Marika M. Holland, David A. Bailey, Kurt A. Refsnider, Scott J. Lehman, John R. Southon, Chance Anderson, Helgi Björnsson, and Thorvaldur Thordarson. Abrupt onset of the Little Ice Age triggered by volcanism and sustained by sea-ice/ocean feedbacks. *Geophysics Research Letters*, 39(2): L02708, January 2012.
- [59] Hermann Harde. Scrutinizing the carbon cycle and CO<sub>2</sub> residence time in the atmosphere. *Global and Planetary Change*, 152:19–26, May 2017.
- [60] Valentina Zharkova. Modern grand solar minimum will lead to terrestrial cooling. *Temperature*, 7(3):217–222, 2020.
- [61] Johann Kepler. *Astronomia nova*. 1609.
- [62] S. K. Stein and T. Elsner. Mean Distance” in Kepler’s Third Law. *Mathematics Magazine*, 50(3):160–162, March 1977.